Analysis of Reaction Products and Conversion Time in the Pyrolysis of Cellulose and Wood Particles

R.S. *MILLER* and 1. BELLAN *Jet Propulsion laboratory California Institute of Technology, Pasadena, CA 91109-8099*

(submitted March 15, 1996)

ABSTRACT—A detailed mathematical model is presented for the temporal and spatial accurate modeling of did-fluid reactions in porous particles for which volumetric reaction rate data is known *a priori* and both the porosity and the Permeability of the particle are large enough to allow for continuous gas phase flow. The methodology is applied to the pyrolysis of spherically symmetric biomass particles by considering previously published kinetics schemes for both cellulose and wood. A parametric study is performed in order to illustrate the effects of reactor temperature, heating rate, porosity, initial particle size and initial temperature on char yields and conversion times. It is observed that while high temperatures and fast heating rates minimize the production of char in both reactions, practical limits exist due to endothermic reactions, heat capacity and thermal diffusion. Three pyrolysis regimes arc identified: 1) initial heating, 2) primary reaction at the effective pyrolysis temperature and 3) final heating. The relative durations of each regime are independent of the reactor temperature and arc approximately 200A, 60°A and 20% of the total conversion time, respectively. The results show that models which neglect the thermal and species boundary layers exterior to the particle will generally over predict both the pyrolysis rates and experimentally obtainable tar yields. An evaluation of the simulation results through comparisons with experimental data indicates that the wood pyrolysis kinet ics is not accurate; particularly at high reactor temperatures.

Key *words:* biomass, cellulose, modeling, porous particle, pyrolysis, wood

NOMENCLATURE

A	Frequency constant.
$c.$	Cellulose.
C	Specific heat.
d	Characteristic pore length scale.
D	Molecular species diffusivity.
e	Specific internal energy.
E	Activation energy.
K	Reaction rate.
M	Molecular weight,

n	Numerical time level.
N	Total number of species.
p	Pressure.
r	Radial coordinate.
R	Radial position.
$\mathcal{R}$	Universal gas constant.
$\dot{S}$	Reaction source/sink term.
t	Time.
T	Temperature.
u	Gas phase velocity.
w.	Wood .
X	Reaction molar fraction.
Y	Gas phase mass fraction.
<>	Solid phase mass average excluding char.

Greek Symbols

Δh	Heat of reaction.
ε	Porosity.
Π	Divergence of the velocity.
λ	Thermal conductivity.
μ	Molecular viscosity.
ρ	Partial density.
$\widehat{\rho}$	True density.
σ	Stefan-Boltzmann constant.
w	Emissivity.

Subscripts and Superscripts

o	Initial value.
c	(onversion.
eff	Effective.
g	Gas phase.
i	Species i.
j	Species j.

p	Particle.
rad	Radiation.
R	Reactor.
s	Solid phase.
t	Total (all species and phases).
T	Thermal.
v	Constant volume.
α	Phase α.
$'$	Excluding char.

1 INTRODUCTION

Solid porous particle combustion (coal, solid waste, solid propellants, etc.) is a subject of wide spread interest for both fundamental research and industrial applications, Modeling of this phenomenon is inherently difficult duc to complexities associated with the multi-phase aspect. Particle porosity, two- and three-phase interactions, and ill-defined boundaries due to solid phase reaction products (e.g. char) need to be considered in a complete model. The combustion of a solid fuel particle can be divided into six primary physical processes:

a) Solid fuel reactions at both the particle surface and the interior.

b) Secondary solid/liquid phase reactions at both the particle surface and the interior.

c) Gas phase reactions both internal and external to the particle.

c) Gas and liquid phase diffusion ("pore diffusion") and/or convection within the particle.

f) Mass transfer with the surroundings.

g) Heat transfer with the surroundings.

"1 he combination of the above processes which determines the combustion characteristics is dependent on the particular reaction of interest. The ratio of reaction to diffusion time scales is in general too small for kinetically controlled models to be effective (see e.g. Di Blasi, 1996b). "Pore diffusion" can control the rate of reaction by limiting the surrounding oxidizer delivery to the particle's interior and/or by cooling the particle's surface due to emerging interior gases, Solid phase fuels may produce additional solid and/or liquid phase products such as char which can act to thermally insulate the particle. In addition, reactions of gas phase species outside of the particle can influence both heat and mass transfer (e.g. exothermic reactions).

Significant early research in this area has been directed at incorporating the above mentioned processes into theoretical models of char combustion and gasification. Early models were limited to analyzing the external particle surface reactions coupled with gas phase transport (Caram & Arnundson, 1977; Mon & Amundson,

1978; Sundaresan & Amundson, 1980). Extensions included the addition of inner-particle diffusion, reaction and pore growth effects (Sotirchos & Amundson, 1984a; Sotirchos & Amundson, 1984b). Further efforts relied on stochastic descriptions of pore distributions and overlap. This latter approach typically employs assumptions of either spherical voids (Loewenberg et. al., 1987), infinite cylindrical voids (Gavalas, 1980; Gavalas, 1981), or arbitrary void sizes and distributions (Bhatia & Perlmutter, 1980; Bhatia & Perlmutter, 198 1). All of the above mentioned models rely on *a priori* knowledge of pore surface regression rates as a function of carbon oxidation and invoke a quasi-steady state assumption for the particle surroundings.

While the above mentioned models have shown some success for modeling char combustion, these approaches arc not directly applicable to other types of solid particle reactions. Reaction rates may occur volumetrically (not only at exposed surfaces) and are more easily measured in this manner in the laboratory. Density changes due to thermal swelling and/or intermediate solid or liquid phase species may cause temporary pore shrinkage. In addition, the presence of gas phase species within the particle results in a nearly uniform diffusion time scale across the particle boundary and a quasi-steady assumption for the particle exterior cannot be justified.

One type of solid reaction which exhibits several of the above characteristics is the pyrolysis of biomass. As biomass is heated in the absence of an oxidizer it produces char, tar and volatile gases. It is now widely accepted that as the heating rate is increased, relative proportions of tar and volatile gases can be increased while producing little, if any, char (Reed et. *al.*, 1980; Diebold, 1980). Fast pyrolysis in the ablation regime has been investigated for wood rods in contact with a hot, spinning disc by Lede *et. al.* (1985) who found that fast pyrolysis is possible when both high heating rates and efficient removal of the reaction products arc present. Possible applications of these processes involve the rapid heating of ground biomass particles (e.g. waste saw dust) in either fluidized beds (Lim *et. al.*, 1995) or vortex reactors (Diebold and Power, 1988) in order to maximize tar and volatile gas yields, The collected gases and tars can be further processed for use in adhesives, resins or for hydrogen fuel production whereas large char yields arc desirable for charcoal production.

The large diversity of biomass feedstock has motivated analyses of the somewhat simplified case of CCIIU1OSC pyrolysis. In general, biomass is composed of approximately 50'% cellulose by mass (Di Blasi, 1993b) and many of the kinetic and hydro/thermo- dynamic processes involved in cellulose pyrolysis may be common to the more general case of biomass. The majority of previous models for both CCIIU1OSC and wood pyrolysis arc based on first order kinetics schemes. These models ***range*** in complexity from one-step global to multi-step kinetics involving both primary and secondary reactions (see Di Blasi (1993b); Antal and Varhegyi (1995) for recent reviews). Only the most recent of these models have attempted to incorporate hydrodynamic and thermodynamic effects. Kothari and Antal (1985) investigated the effects of heatup time and devolatilization time on the flash pyrolysis of cellulose. They found that time delays and endothermic reactions place practical limits on attainable particle

temperatures. Simmons and Gentry (1986) studied the kineticall y controlled regime of the cellulose pyrolysis of sub-millimeter sized particles. Using a mathematical model with prescribed particle surface conditions, they were able to make predictions of the range of kinetic control as a function of particle size and heating temperature. Poor comparisons with experiments were attributed to neglect of the external thermal boundary layer in the mode]. Di Blasi (1994) extended the kinetics scheme of Bradbury *et.* al. (1979) to include secondary reactions of volatiles to simulate the pyrolysis of cellulose slabs. The model accounts for both heat and mass transfer within the slab through an equation for internal energy and Darcy's law for the gas phase velocity, and has been extended to multi-step kinetics for wood pyrolysis (Di Blasi, 1992; Di Blasi, 1993a). The model is applicable only within the slab and the particle surface conditions arc assumed functions of the reactor temperature. However, effects "on pyrolysis due to the thermal boundary layer and chemical reactions outside of the particle can become significant and have recently been connected to the wide variation of kinetic parameters measured in experiments (Narayan and Antal, 1996).

The objective of this paper is to present a model of solid particle reactions which is sufficiently robust to incorporate all of the above listed physical processes both internal and external to the particle, and which is applicable to volumetric reaction rate data, In particular, no quasi-steady assumption is made for the particle surroundings, and the particle surface conditions arc allowed to evolve in a "natural" manner determined by the far field temperature and pressure. The model is then applied to example cases of spherically symmetric cellulose and wood particle pyrolysis in an initially quiescent environment of high temperature steam. The effects of reactor temperature, heating rate, initial particle size, initial porosity and initial particle temperature on both char formation and conversion times are investigated. A comparison of the simulated results with experimental data is made and is discussed in evaluating the accuracy of the assumed kinetics schemes. The paper is organized as follows: Section 2 presents the general model equations together with the kinetics schemes and properties for both cellulose and wood reactions. Numerical solutions and a parametric study are presented in Section 3 along with discussions of char yields, conversion times, spatial tar distributions and Comparisons with experiments. section 4 is devoted to conclusions and further discussions.

2 THEORETICAL FORMULATION

Consider a single porous solid particle having both a porosity (ratio of pore volume to total volume) and a permeabil it y sufficientl y large to allow for continuous gas flow. Assume that the particle is allowed to react and that only volumetric reactions arc known. In this case, a dct'ailed analysis of the internal pore structure is superfluous because only the bulk "effective" proper-tics of the porous material arc needed. We allow for the general case in which both liquid and gaseous reaction products may be formed; however, both convection and

diffusion of the liquid arc neglected. This last assumption is justified provided that either the viscosity of the liquid is substantially larger than that of the gases or the reaction time scale of the liquid is much smaller than its convection and diffusion time scales.

2.1 *Governing equations*

The governing equations for the solid particle dynamics are presented in spherically symmetric form; the extension to muhi-dimensions being straight forward, A combination of two perspectives is employed to describe the particle dynamics. In the first approach, the various species and phases within the particle are viewed as a "mixture. " In this case, it is the partial densities which arc relevant. We denote partial densities as $\rho_{\alpha,i}$ and true densities as $\widehat{\rho}_{\alpha,i}$, where the subscripts denote both the phase [$\alpha =$ s (solid or liquid), g (gas)] and the species ($i = 1, \ldots N$; where N is the total number of species). Note that the above assumptions imply that solid and liquid phase species are treated identically. The mass conservation equation for the solid phase species is:

$$\frac{d\rho_{s,i}}{dt} = \dot{S}_{s,i}, \tag{1}$$

where the appropriate source/sink terms due to reactions arc contained in $\dot{S}$ (subscripts as defined above) and both convection and diffusion are neglected. In similar fashion, the gas phase continuity equation is:

$$\frac{\partial \rho_g}{\partial t} + \frac{1}{r^2}\frac{\partial}{\partial r}\left(r^2 \rho_g u\right) = \dot{S}_g \tag{2}$$

where the radial coordinate is r, the radial velocity component is u, the gas phase partial density is $\rho_g = \sum^g \rho_{g,i}$ and the corresponding source term is $\dot{S}_g = \sum^g \dot{S}_{g,i}$ (the summation $\sum^\alpha$ denotes a sum over all species of phase α). So far, the porosity of the particle (ε) only appears indirect] y through the relation between the partial and true densities:

$$\rho_g = \varepsilon \widehat{\rho}_g, \qquad \rho_{s,i} = (1 - \varepsilon)\widehat{\rho}_{s,i}, \tag{3}$$

$$\varepsilon = 1 - \sum^s \rho_{s,i}/\widehat{\rho}_{s,i}. \tag{4}$$

In general, the true densities of the solid phase species arc described through additional equations of state; however, for the purpose of the present work they are assumed to have prescribed constant values, By definition, the porosity is based only on the gas phase volume whereas the stationary medium includes both the solid and the liquid phases.

The above equations arc coupled through both source terms and additional equations for species, momentum and energy conservation, along with an appropriate equation of state for the gas phase. The species conservation equations arc formulated in terms of the gas phase mass fraction Y_i ($\sum^g Y_i = 1$):

$$\frac{\partial \rho_g Y_i}{\partial t} + \frac{1}{r^2}\frac{\partial}{\partial r}\left(r^2 \rho_g Y_i u - r^2 \rho_g \mathcal{D}^{(i)}_{eff}\frac{\partial Y_i}{\partial r}\right) = \dot{S}_{g,i} \tag{5}$$

The species diffusion is assumed to be Fickian with an effective molecular diffusivity $D_{eff}^{(i)}$ due to porosity effects. Following classical porous media theory and empirical measurements, the effective diffusivity is assumed to be proportional to the porosity and is modeled as $D_{eff}^{(i)} = \varepsilon D^{(i)}$ where $D^{(i)}$ is the molecular diffusivity of species i (Bear, 1972). In general, the porosity is represented by a rank two symmetric tensor to properly describe anisotropic pore distributions; however, only locally isotropic porosities and diffusivities are considered in the current work as more precise information is not available.

The conservation equation for the gas phase momentum is modeled through a "channel" description (second perspective), *i.e.* as a mixture of gases flowing through individual "channels" (pores) within the particle:

$$\frac{\partial \rho_g u}{\partial t} + \varepsilon \left[\frac{\partial}{\partial r} \left(\rho_g u^2 \right) \right] = -\frac{\partial p}{\partial r} + \frac{1}{r^2} \frac{\partial}{\partial r} \left[r^2 \mu_{eff} \left(2 \frac{\partial u}{\partial r} - \frac{2}{3} \mathrm{II} \right) \right] + \frac{4}{3} \frac{\mu_{eff} \mathrm{II}}{r} - 4 \frac{\mu_{eff} u}{r^2} \tag{6}$$

where the velocity divergence is:

$$\mathrm{II} = \frac{1}{r^2} \frac{\partial}{\partial r} \left(r^2 u \right), \tag{7}$$

the pressure is p and the effective molecular viscosity is μ_{eff}. The fully compressible form of the momentum equation is employed, as a source term in the continuity equation results in non-zero divergence of the velocity field. The effective viscosity is modeled in a similar manner as the diffusivity; however, the values of the gas species' molecular viscosities ($\mu^{(i)}$) are locally mass averaged to account for mixture effects:

$$\mu_{eff} = \varepsilon \sum^{g} Y_i \mu^{(i)}. \tag{8}$$

Although the gas diffuses according to the effective viscosity relation, additional drag forces are experienced by a flow convecting through a porous medium. These effects are due to the geometry of the voids and to viscous shear stresses along solid-gas boundaries. In order to avoid a complicated analysis of the pore geometry, these effects are lumped together and modeled by "damping" the convective terms in the momentum equation proportional to the porosity. This damping is somewhat arbitrary, yet appears to be reasonable under the previous restriction of relatively large porosity ardor permeability. The above momentum equation offers several advantages over the traditional use of Darcy 's Law which states that the velocity is proportional to the product of the pressure gradient and the permeability. Equation (6) is derived theoretically and with relatively few, and known, assumptions. It is valid for both the interior and the exterior of the particle and takes full account of transient effects. Darcy's Law is completely empirical and has not been correlated for the case where gas phase sources occur within porous media, nor for flows in which transient effects are important (Bear, 1972).

The temperature is obtained through a "mixture" modeled conservation equation for the internal energy, Local thermal equilibrium is assumed for all species and phases ($T = T_i$, all i). All species are assumed calorically perfect such that the partial internal energy (e_i) is proportional to the specific heat at constant volume; $e_i =$

$\rho_i C_v^{(i)} T$. With this notation, the gas phase partial internal energy is:

$$e_g = \rho_g \left(\sum^{g} C_v^{(i)} \right) T, \tag{9}$$

and the total internal energy is:

$$e_t = e_g + \left(\sum^{s} \rho_{s,i} C^{(i)} \right) T, \tag{lo}$$

where $C_v^{(i)}$ is the constant volume specific heat of gas phase species i, and $C^{(i)}$ is the specific heat of either solid or liquid phase species i. With this notation, the total internal energy is governed by:

$$\frac{\partial e_t}{\partial t} + \frac{1}{r^2}\frac{\partial}{\partial r}\left[r^2 e_g u - r^2 \lambda_{eff} \frac{\partial T}{\partial r} \right] = p\Pi + \sum \dot{S}_i \, \Delta h_i \tag{11}$$

where Fourier conduction with effective thermal conductivity λ_{eff} is assumed, only gas phase energies are allowed to convect and viscous dissipation is neglected. The last term on the right hand side (*rhs*) represents a summation over all reactions which accounts for both heat release and/or phase changes with heats of reaction A hi. Modeling the effective conductivity is more complex than the previous transport properties due to the fact that heat transfer occurs simultaneously through all phases and species. We choose to model the multi-phase heat transfer in terms of a *parallel conduction* model inspired by previous empirically tested models of two-species conduction in porous media (Bear, 1972):

$$\lambda_{eff} = (1 - \&) \left\{ \frac{\sum^{s} \rho_i \lambda^{(i)}}{\sum^{s} \mathrm{Pi}} + \lambda_{\mathrm{rad}} + \varepsilon \sum_{1}^{g} Y_i \lambda^{(i)} \right. , \tag{12}$$

where $\lambda^{(i)}$ is the thermal conductivity of species i. Gas phase species are assumed to be transparent to radiation while the solid and liquid phase radiation are modeled as in Chan *et. al.* (1988) with an effective conductivity: $\lambda_{\mathrm{rad}} = \sigma T^3 d/\omega$, where $\sigma = 5.67$ x 10-1' $kJ/m^2 sK^4$ is the Stefan-Boltzmann constant, ω is the emissivity and d represents a characteristic length scale for the pore size. The above model quantifies a "flow" of heat simultaneously (in *parallel*, implying volume averaging) through both the solid and gas phases, where individual species conductivities are mass averaged among species of the same phase. While other conduction models have been proposed (e.g. *series* and combinations of *series-parallel*), all are at best intuitive and compare similarly with experiments (Bear, 1972).

The above set of governing equations is completed by an equation of state. The total pressure driving the gases is assumed to be related to the temperature and density through the perfect gas law:

$$p = \frac{\rho_g}{\varepsilon} \left(\sum^{g} Y_i / M_i \right) \overline{R} T, \tag{13}$$

where M_i is the molecular weight of species i and $\overline{R}$ is the universal gas constant. The presence of the porosity in the equation of state indicates that the pressure is related to the "true" gas density $\hat{\rho}_g$. Equations (1)-(13) describe the essential physical processes of reactions in porous solid particles with multi-species/phase interactions. They

arc valid for both the interior and the exterior ($\varepsilon \rightarrow 1$) of the particle and provide a fully transient description of the particle behavior with relatively fcw assumptions.

2.2 *Biomass pyrolysis*

The equations derived in Section 2.1 are applied to the pyrolysis of both cellulose and wood particles by implementing the kinetics schemes compiled by Di Blasi (1994) and Di Blasi (1993a), respectively. The two reaction schemes both employ a simplified decomposition of the primary solids to form three lumped product groups; solid char, tar vapors and low molecular weight gas (Fig. 1). The cellulose is additionally considered to pass through an intermediate solid form labelled active cellulose. All of the reactions arc first order, irreversible and follow Arrhenius temperature dependencies of the form $K_i = A_i \exp[-E_i/\bar{R}T]$ where K_i is the reaction rate, A_i is the rate frequency constant, E_i is the activation energy and the subscript refers to the reacting species. The reaction rates arc applied to the particle model to form source terms of the form:

$$\dot{S}_i = -\rho_i K_i, \qquad \dot{S}_j = +X_j \rho_i K_i \tag{14}$$

for the reaction of solid phase species i ($\dot{S}_i$) with corresponding production of species j ($\dot{S}_j$) and X_j is the molar fraction (note that there is no summation over repeated indices throughout the paper). Similar forms for the gas phase reactions arc in terms of the partial densities. Values of the activation energies, rate constants and heats of reaction are provided in Table 1. Reaction K_2 is assumed to produce both char and gas in the respective ratios of 0.35 and 0.65 and all remaining X_j arc equal to unity. All solid phase reactions, with the exception of the primary cellulose decomposition arc endothermic while secondary gas reactions are exothermic. The reaction frequencies for the wood pyrolysis are consistent with the original values as calculated by Thurner and Mann (198 1). The frequency constants for the primary wood reactions used in Di Blasi (1993a) appear to bc larger than the originals by a factor of 3600; we were informed that this was a modification made by the author (Di Blasi, 1996a) to duplicate experimental char densities. Implications of this modification will be discussed below,

The particles considered in this work are initially at equilibrium in an environment composed of inert superheated steam. All material properties arc taken from the compiled data of Di Blasi (1 994) and Di Blasi (1993a) for the reacting species, while the H_2O properties are from appropriate steam tables. The wood kinetics and reactions were originally compiled from several sources and do not correspond to any specific wood type. Tables 2 and 3 contain the solid and gas phase properties, respectively. The steam data is taken at a reference pressure of $p = 100kPa$ and temperature of $T = 500K$, and unavailable gas properties arc assumed to bc the same as the steam. All of the true solid densities are defined in terms of the initial porosity of the material. There arc two advantages to this approach. First, experimental measurements of the true density are very difficult, whereas the apparent, or partial, density is relatively simple to measure. Second, with the density definition employed here,

the initial porosity may be varied in order to study its influence without altering the total mass of the particle. The true density of char is assumed to be the same as the corresponding primary reactant. The emissivity is taken to be w = 1 and the radiation length scale is $d = 4.0 \times 10^{-5} m$ taken from Chan *et.al.* (1988).

2.3 *Turbulence considerations*

The equations presented above do not include a turbulence model. Although the particles are assumed to be initially located in a quiescent environment, significant gas phase velocities can result in turbulent diffusion around the particle. This could result in three primary alterations to the particle surroundings: 1) Increased temperature gradients near the boundary can increase the total heat flux to the particle. 2) Enhanced mixing of gas phase reactants can significantly increase the rate of chemical conversion near the particle for diffusion flames. 3) Turbulent diffusion of the gases can change the spatial distributions of exothermic reactions and therefore indirectly affect the particle heating rate. Neglect of a turbulence model for the present biomass pyrolysis is considered to be justified in regard to 2) and 3) because only first order reactions are considered (non-diffusion limited) and only mildly exothermic heats of combustion are involved. In regard to issue 1), the present study treats the thermal radius, and therefore the heating rate, as a free parameter. These considerations combined with *a* posterior analysis of the simulation results indicate that the neglect of a turbulence model is justified for the present biomass particle pyrolysis.

2.4 *Initial conditions, boundary conditions and the thermal radius*

A particle of initial radius $R_{p,0}$ and uniform temperature $T_{p,0}$ is exposed at time $t = 0$ to a quiescent environment composed of super-heated steam. Numerical solutions are obtained for the spherical 1 y symmetric domain within the interval $[0, R_R]$ where the outer domain radius, R_R (referred to as the reactor radius), corresponds to the reactor conditions. Symmetry conditions are employed at the inner domain boundary; i.e. $u = 0$ and $\partial/\partial r = 0$ for all remaining variables. We model the exterior boundary in a manner similar to the "sphere of influence" (S01) approach of Bellan and Cuffel (1983) which was originally proposed to account for thermodynamic interactions among liquid droplets in sprays (clusters). The SOI represents a characteristic length scale for these interactions and corresponds to the radius of a fictitious sphere located at the droplet center. This radius, R_R, is equal to one half the mean droplet center separation. The proper boundary conditions at $r = R_R$ are obtained by matching the temperature and pressure (and therefore the density) to the local reactor conditions while assuming that $\partial/\partial r = 0$ for all remaining variables. R_R is a function of both the local number density and the three dimensional pricking factor. We extend the original SOI concept to introduce a "thermal radius" $R_T \leq R_R$ which is defined such that the temperature is held constant and equal to the local reactor conditions, i.e. $T = T_R$, for all $r \geq R_T$. In this manner, the effective heat flux received by the particle can be altered independently of the reactor temperature

while resolving gas phase reactions exterior to the particle. The results presented in the following section arc obtained for a single particle and a fixed normalized reactor radius $R_R = 10 R_{p,0}$ with constant reactor pressure $p = 100 kPa$. In addition to other quantities, both the reactor temperature and the thermal radius are varied in order to independently study the effects of the heating temperature and the heating rate, respectively.

2.5 *Solution procedure*

The modeled equations are solved numerically utilizing a procedure based on finite difference approximations for both spatial and temporal derivatives. All convective and first order derivatives are approximated via upstream differences in order to maintain proper ellipticity of the equation set, while diffusion second derivatives are seeond order central. Acoustic waves are filtered through use of a semi-implicit iterative pressure solver. The basic method is as follows: The solid phase density, gas mass fraction and internal energy equations are integrated one time step (from time level n to n + 1) using an explicit forward time difference. These values give an approximation for the gas phase density and all necessary properties at time level $n + 1$. A predictor value of the velocity is then calculated from the gas phase continuity equation. Next, the pressure is obtained by solving a Poisson equation obtained by taking the divergence of the momentum equation. The pressure is then used to correct the gas density and the process is repeated until convergence is achieved. All simulations are performed with a compressed and staggered 64 grid point spatial resolution of the radial coordinate with compression increasing towards the origin such that 21 grid points are within the initial particle boundary. Sixty eight simulations were performed on a Cray-YMP supercomputer requiring a total central processor time of approximately 50 hours.

3 RESULTS

Before proceeding with a parametric study it is informative to illustrate the particle evolution through a “baseline case” simulation for both cellulose and wood and to compare their behavior. The baseline case conditions are: $T_{p,0} = 500K, T_R = 900K, R_T = 5R_{p,0}, R_{p,0} = 5mm$ and $\varepsilon_0 = 0.7$. The simulation is terminated at a final time t_c (the conversion time) at which the remaining solid mass, minus the char, has reached 0.l% of the initial particle mass. ‘he conversion times for the cellulose and wood simulations arc $t_c = 253.7$s and $t_c = 347.8s$, respectively.

Figure 2 depicts the temporal evolution of the partial char density for both cellulose and wood. in both cases, no char exists initially. The small amount of char forming outside of the radial position $R_{p,0}$ is due to the necessary smoothing of the initial particle gradients for numerical resolution across the outer boundary of the particle. As the particles are exposed to the high temperature steam environment, heat diffusion into the particle results in a pyrolysis wave having a thickness $\sim 1mm$ which travels radially inward producing solid char residue. Approximately six times more char by mass is formed by the wood reaction than by the cellulose. The

final porosity values are nearly uniform within each of the particles; however, the average values differ and are $\varepsilon(t = t_c) \approx 0.98$ and $\varepsilon(t = t_c) \approx 0.91$ for cellulose and wood, respectively. The smaller final char densities near the origin are due to biomass remaining at the termination of the simulations.

As the pyrolysis wave travels through the particle, both tar vapors and gas arc produced from the reacting solids and, due to pressure gradients, are ejected from the particle. The production of both tar and gas drives the inert steam out of the pores and away from the particle. Figure 3 indicates that the maximum tar mass fractions are located within the particle. In this region, the tar fraction maintains a nearly uniform value duc to near uniform temperatures and reaction rates within the particle (discussed below). In addition, the slightly larger tar mass fractions observed for the cellulose particle indicate that the effective production rate of tar is larger for cellulose than for wood. As tar is ejected, it encounters the hot environment resulting in increased conversion rates to gas. In fact, for both cellulose and wood, nearly all of the tar is converted to gas within the range $r \leq 5R_{p,0}$. This range therefore represents the effective range for which exterior gas phase reactions may influence the pyrolysis evolution due to exothermicity. The rapid tar decomposition near the particle has consequences for experimentally obtainable pyrolysis product measurements and is discussed in more detail below.

The temporal evolution of the temperature profiles can provide insight into the importance of the outer particle regions in affecting the pyrolysis process. Figure 4 illustrates this effect for both cellulose and wood. The high temperature environment maintains relatively large temperature gradients at the particle surface, whereas endothermic reactions smooth the internal thermal gradients. These competing processes result in a relatively thin reaction zone located at the particle surface. The final core temperature for the wood particle is larger than that corresponding to the cellulose particle despite the larger mass (with the same endothermic heat of reaction) of the wood particle. This is a result of the smaller reaction rate of the wood particle as can be deduced from the above listed conversion times. The slower wood reactions absorb heat endothermically at a lesser rate than the cellulose; thus allowing for thermal diffusion to heat the particle to larger temperatures, Examination of Fig.4 reveals that the actual particle surface temperature never reaches the reactor temperature T_R. In fact, during the majority of the conversion, the particle surface temperatures are $\sim 200K$ less than T_R. Analysis of the surface temperature indicates that its rate of increase with time cannot accurately be modeled as a linear function . These results suggest that pyrolysis models which neglect the outer particle thermal boundary layer may substantially over predict the reaction rates.

Pressure gradients resulting from the conversion of solid to vapor produce maximum gas phase velocities at the location of the pyrolysis front (Fig.5). Convection carries endothermically cooled interior tar and gas out of the particle and thus aids in maintaining a relatively low particle surface temperature. The magnitudes and relative profiles of the interior velocities are in general agreement with the cellulose pyrolysis simulations

based on Darcy's Law by Di Blasi (1994). Outside of the particle there arc no gas phase mass sources and the velocities decay roughly as r^{-2}. The cellulose actually yields a larger maximum velocity than the wood although it produces substantially less gas phase species by mass. This is because the velocity is related to the reaction rate which is larger for cellulose. Analysis of these results along with others not shown here indicates that an outer computational radius of $10R_{p,0}$ is sufficient to capture the pertinent physics of the particle pyrolysis without significant artificial boundary effects. In addition, due to the complete conversion of tar to gas within the computational domain, further discussions are primarily limited to char yields with the caveat that the remaining products are converted entirely to the gas species within the particle's near field surroundings. However, in order to provide insight into the role of the exterior gas phase reactions, a discussion of spatial tar distributions as a function of the reactor temperature is provided in Section 3.1.3.

3.1 Effects of the reactor temperature

in this section, the focus is on the values of the conversion times and on the final char yields. Knowledge of the final char yields is necessary in order to either maximize or minimize char formation depending on the particular application; e.g. charcoal or volatile gas production, respectively. On the other hand, conversion times dictate the types of reactors and residence times which arc capable of producing the desired yields. The most obvious parameter influencing both t_c and the pyrolysis products is the reactor temperature. Thus simulations arc conducted for both particle types for $600K \leq T_R \leq 1500K$ with all other parameters equal to the baseline case values ($R_T = 5R_{p,0}, R_{p,0} = 5mm, \varepsilon_0 = 0.7$ and $T_{p,0} = 500$ K). The conversion times and char yields are presented in Fig.6 for both cellulose (c.) and wood (w.). For both particles, the most substantial effects of the reactor temperature occur for relatively low ambient temperatures. A "transition" value of the reactor temperature, $T_R \sim 700K$, appears to separate two regimes of pyrolysis behavior. The value $700K$ is not meant to quantify a precise transition temperature but is only listed as an apparent range for which the observed changes occur, Below this value, the conversion times increase rapidly with decreasing reactor temperatures (from minutes to hours). The char yield for the cellulose particle also shows a relatively sharply increasing trend in this region. The wood particle shows a nearly constant char yield of ≈ 0.32 for all reactor temperatures; however, the char yields decrease slightly for $T_R < 700K$. On the other hand, for $T_R > 700K$ only relatively mild variations of both the char yield and the conversion time arc observed for both particles.

3.1.1 *Kinetic limitations*

'I he pyrolysis trends observed in Fig.6 arc best explained in terms of two competing processes; 1) reaction kinetics and 2) "thermal inertia." Kinetics dictate the limitations imposed on pyrolysis due to reaction rates, whereas thermal inertia accounts for limitations imposed on both the particle temperature and its rate of increase

due to diffusion, heat capacity and endothermic solid reactions. If the ratio of the thermal diffusion time scale to the reaction time scale << 1, then particle pyrolysis occurs in the kineticall y controlled regime. The particle temperature is instantaneously raised to the reactor temperature and any variations duc to exothermic/endothermic reactions are smoothed by diffusion infinitely fast. Under these conditions, it is possible to define both a kinetic char limit and a kinetic conversion time limit for the reactions, both being functions of T_R only. Table 4 lists the definitions of these limits for both cellulose and wood pyrolysis where the reaction rates (K_i) are evaluated at $T = T_R$. The conversion time is evaluated as that corresponding to a residual mass of 10-3 which makes the definition independent of the initial particle size or mass. The time to convert raw cellulose to the active form has been neglected as being much smaller than the remaining reaction times, and secondary char production has been included for wood pyrolysis.

Figure 7 presents the kinetic limits on char yields and conversion times for both cellulose and wood pyrolysis as a function of T_R. The limiting values of the conversion times are observed to be strong functions of the reaction temperature. Complete pyrolysis at the kinetic limit can require anywhere from weeks to micro-seconds within the range of reactor temperatures in current use. For all practical ranges for which char production is to bc minimized (large T_R), the wood reaction is always slower than the cellulose reaction. It is well known that commercial processes which aim at maximizing char yields generally employ long residence times with low final heating temperatures. For example, char yields as high as 50% have been reported from the pyrolysis of bagasse at $530K$ with 65 hour heating times (see e.g. Antal and Mok, 1990). The kinetic char yield limit for cellulose pyrolysis is in good qualitative agreement with these observations since the yield decreases monotonically with reactor temperature. However, the wood reaction shows a peak char yield at $T_R \approx 650K$ with a relativel y sharp drop in yield below this temperature. This apparent contradiction with experimental observation may indicate a flaw in the wood pyrolysis kinetics scheme.

In order to quantify the relative ratio of the kinetically controlled and the diffusion controlled pyrolysis regimes, it is convenient to define two kinetic "efficiency" factors. Both a yield efficiency and a conversion efficiency are defined as the ratio of the kinetic limit to the actual simulation value of the final char yield and the conversion time, respective] y. Values of these ratios which approach unity indicate the kinetically controlled regime, whereas ratios approaching zero indicate strongly diffusion controlled pyrolysis, Both ratios must be in agreement as a yield efficiency of unity alone is not sufficient to conclude kinetically controlled pyrolysis. Both efficiency factors arc illustrated in Fig.8 as a function of T_R. It is apparent that diffusion effects are substantial throughout the entire range of temperatures considered. Only as T_R is decreased below $600K$ and conversion times become on the order of hours and larger can biomass pyrolysis truly bc considered to bc kinetically controlled. In the case of wood pyrolysis, kinetically controlled predictions of product yields may give reasonable results, even though

the conversion times indicate that diffusion effects are strong. This is an artifact of the present kinetics scheme for wood pyrolysis which yields only mild variations in char yield with reaction temperature. The quantitative results presented thus far are valid only for the particular particles under consideration and are expected to be functions of particle size and heating rate in addition to other properties (conductivities, heats of reaction, *etc.*).

3.1.2 *Effective pyrolysis temperature*

A comparison of the results of Figs.6 and 7 suggests that the simulated pyrolysis of both cellulose and wood is occurring within a relatively narrow effective reaction temperature range slightly larger than $600K$. This hypothesis is confirmed by examining the mass averaged particle temperature:

$$< T_p >= \frac{\int_0^\infty 4\pi r^2 \rho_s' T' \cdot dr}{\int_0^\infty 4\pi r^2 \rho_s' \cdot dr}, \tag{15}$$

where ρ_s' indicates the partial solid phase density *excluding the* char. Figure 9 depicts the mass averaged particle temperature evolution as a function of nondimensional time for several values of the reactor temperature in the range $[700K, 1200K]$. The curves arc almost identical for both cellulose and wood when time is normalized with t_c. Examination of the mean particle temperature indicates three primary phases of evolution for both cellulose and wood pyrolysis: 1) An initial rapid increase in temperature as heat diffuses into the particle from the surroundings. 2) A primary reaction regime at a nearly constant "effective pyrolysis temperature" during which endothermic reactions strongly resist any further particle heating. 3) A secondary reaction regime within which only relatively small particle mass remains and the total heat loss due to reactions is significantly smaller than heat diffusion into the particle. The majority of the pyrolysis occurs in the primary regime within which the particle temperatures for both cellulose and wood are limited to values in the range of approximately $(600K, 650K)$. Only relatively small variations of char yield and conversion time can bc expected for reactor temperatures above this range, The behaviors associated with regimes 1) and 2) arc in agreement with the numerical results of flash CC1IU1OSC pyrolysis by Kothari and Antal (1985) obtained using a much simpler particle model. Their results indicate a larger maximum particle temperature than Fig.9 indicates; approximately $775K$ for particle diameters $\leq 0.5mm$. However, these particles may have a mass too small for the endothermic heat absorption to overcome the inward thermal diffusion. The present results indicate that the effective pyrolysis temperature is determined primarily by the magnitude of the primary reaction endothermicity, the particle mass and the reaction rate: The pyrolysis temperature is therefore not directly related to kinetic and diffusion reaction limits.

Further evidence for the three pyrolysis regimes is found in Fig. 10 which depicts the particle heating rate as a function of both nondimensional time and T_R'. For the purpose of this study, the heating rate is defined as the time derivative of $< T_p' >$. This definition is appropriate for the current discussion because the endothermic reactions maintain a fairly uniform temperature profile within the solid and the spherical mass averaging of the temperature

gives a larger "weighting" to the actual pyrolysis temperatures near the particle surface (the nonlinear temporal dependence of the surface temperature was discussed above). In addition, this definition eliminates any ambiguity in prescribing the location of the particle surface and also neglects contributions from residual char regions left behind the pyrolysis wave which no longer influence the temperature via endothermicity effects. Figure 10 clearly reveals the three pyrolysis regimes as distinguished by regions of; 1) relatively large positive, but decreasing, heating, 2) virtually zero heating rate when inward thermal diffusion balances endothermic absorption, and 3) positive and increasing heating rates when the particle mass has become too small for endothermic reactions to prevent the particle temperature growth. Both Figs.9 and 10 suggest that the relative durations of the pyrolysis regimes (with respect to t_c) appear to be independent of the reactor temper-ature and arc approximately 20%, 60% and 20%, respectively. The heating rates in the normalized time frame are almost identical except for early times when large reactor temperatures result in increased heat fluxes into the particle. In general, the heating rates are always less than 10K/s (a factor of ten larger than reactor heating rates used in traditional TGA experiments; e.g. Bilbao *et. al.*, 1992) and their functional dependence on time is highly nonlinear.

The presence of the three regimes is not always readily apparent. For example, Bilbao *et.al.* (1992) studied the effect of the reactor heating rate on the thermal decomposition of spherical pine particles in the size range $4.0cm \leq R_{p,0} \leq 11.2cm$. hey presented experimentally obtained results for the temporal dependence of the particle temperature for various radial positions inside of the particle. The initial particle masses are relatively large and thus endothermic heat absorption should be substantial; however, only the particle core temperatures exhibit the primary pyrolysis regime (as observed by intervals of near constant temper-ature). The reason for this apparent discrepancy is twofold: First, the experimental measurements for outer radial positions do not consider that the pyrolysis front passes through these positions, leaving behind only char with no further endothermic reactions to balance thermal diffusion. Second, the experiments considered particles which began in a "cold" reactor which was slowly heated to the final reactor temperature (from $303K$ to 923K at rates $\leq 12K/\min$). Examination of their data shows that nearly 50% of the pyrolysis is complete before the reactor temperature reaches $700K$, even for the largest particle size and heating rote. The primary reaction regime will only be easily distinguishable when the reactor temperature is significantly larger than the effective pyrolysis temperature. This is indeed the case for the results of Figs.9 and 10 in which the reactor temperature is constant and $T_R \geq$ 700K

3,1.3 Tar distributions

Important issues arc the accurate measurement of tar yields and whether tar yields increase at a constant rate with increasing reactor temperature.

The general form of the tar profiles was demonstrated in Fig.3 and in the corresponding discussions. Another consequence of the rapid depletion of tar in the particle's vicinity is its influence in the experimental analysis of

pyrolysis vapor yields. The typical experimental method of vapor collection is to rapidly quench the gas phase species in order to hault the reactions and to therefore achieve representative samples of the various species yields. For example, Scott *et. al.* (1988) measure both cellulose and wood pyrolysis products using a "cryovortactor" which quenches the gas phase products via injection of a turbulent stream of cryogenic nitrogen immediately after the pyrolysis. Accurate measurements of the true product yields are only possible when the time lag between pyrolysis and quenching is much smaller than the tar conversion time scale. The results presented previously in Fig.3 suggest that the sample measurements may vary substantially from the actual exit yields due to rapid gas phase reactions occurring in the immediate vicinity of the particle.

An examination of the tar distribution within the particle surroundings provides a qualitative analysis of the limitations on gas phase pyrolysis measurements as caused by tar decomposition near the particle. Figure 11 presents both the maximum normalized radius at which the tar mass fraction has decayed to 0.05 (the "5% *tar* radius") and the maximum tar mass fraction for both CC1IU1OSC and wood as a function of the reactor temperature ("maximum" indicates for all times). Radial values $> 10R_{p,0}$ indicate that the 5°/0 radius is located exterior to the computational domain. All of the actual tar profiles arc of the same general form as those previously shown in Fig.3. These two parameters provide a measure of how closely to the particle the tar is distributed and how much tar is produced, respectively. The **5°/0 tar** radius and the maximum tar fraction show opposite dependence on the reactor temperature. Figure 11 indicates that as the reactor temperature is increased, the tar evolves an increasingly narrower distribution adjacent to the particle surface. On the other hand, the maximum tar (at the surface and interior to the particle) increases as the reactor temperature is increased. These observations have important consequences to both experiments and commercial reactors,

Figure 11 suggests that experimental mcasurcmcnts may under predict the actual tar yields which exit the particle as further tar decomposition occurs both rapidly and near to the particle. This argument can be used to explain the results of Di Blasi (1996b) who used a numerical pyrolysis model, based on the same cellulose kinetics scheme as employed in this paper, to predict the tar, gas and char yields measured by Scott et, al. (1988) in the "cryovortactor." The Di Blasi model does not include reactions in the outer particle domain and the total tar yields correspond only to the total tar exiting the particle surface. The numerical model was applied for a nearly kinetically controlled particle size in an attempt to duplicate the experimental conditions. Comparisons showed good agreement for the total char yield predictions; however, with significant over prediction of the total tar yields, Further tar decomposition may have occurred outside of the particles before the cryogenic nitrogen stream could quench the reactions. In this case, it would be expected that a pyrolysis model which neglects the particle surroundings would display the above trends. That is, an over prediction of experimental tar yields, even if the kinetics scheme is accurate and the total char yield is well predicted.

The results of Fig. 11 also indicate that there exists an optimal temperature for applications which aim at maximizing tar yields (e.g. biomass pyrolysis for commercial hydrogen production). Although increasing reactor temperatures produce increasing total tar yields, the relatively narrow distributions of the tar near to the particle surface limit the effective tar yields which can be hru-vested. Caution must bc exercised in raising the reactor temperaturc because the quenching of the pyrolysis products may not be fast enough to capture the increased tar productions, In this case the added expense of heating the reactor to large temperatures may not only be costly, but may actually yield less tar than a lower, and less expensive, optimal reactor temperature. The present model is capable of predicting such optimal reactor temperatures. Experimental measurements of optimal tar producing reactor temperatures as a function of both the reactor type and the biomass feedstock are needed to validate the predictions.

3..? Effects of additional parameters

In order to make useful predictions of biomass pyrolysis, it is necessary to extend the results of the previous section to include the effects of R_T (heating rate), $R_{p,0}, \varepsilon_0$ and $T_{p,0}$. As the variation of each parameter is studied, the remaining parameters are kept constant and take the baseline case values; $T_R = 900K, R_T = 5R_p$, $R_p = 5mm, \varepsilon_0 = 0.7$ and $T_{p,0} = 500K$. The kinetic limits on yield and conversion time are not dependent on *these* parameters. As such, the efficiency factors are inversely proportional to the proceeding simulation results. Therefore, quantitative values for these factors are only discussed intermittently and when pertinent; however, the efficiency magnitudes can be calculated from the data provided in Table 4. In addition, the parameters studied in this section show significantly less influence on the tar distribution than did the reactor temperature. As such, tar distributions are no longer discussed; however, we note that with $T_R = 900K$ all of the cases considered in this section are characterized by total tar decomposition within the simulated domain.

3.2.1 Effects of the thermal radius

Heating rates arc known to strongly influence biomass pyrolysis yields and evolutions (see e.g. Antal and Mok, 1990). Previous numerical investigations which address this issue have been restricted to models which either mode] the particle surface conditions or which usc steady state assumptions for the particle surroundings (see e.g. Di Blasi, 1993a). Variations in the heating rate within experimental and commercial reactors arc difficult to model quantitatively. In addition to T_R, the heating rate is determined by many factors. For example, free stream velocities, turbulence intensity, contact with solid surfaces and clustering of the biomass particles within the reactor may all strongly affect the heating rate each particle experiences. Therefore, for the purpose of the present work, effects due to the heating rate are studied only in a qualitative manner by varying the thermal radius, R_T.

The final time char yields and conversion times for the biomass particles are presented in Fig. 12 for thermal radii in the range $1.15 \leq R_T/R_{p,0} \leq 10$. The largest effect of the heating rate is observed in the variations of the conversion times for both cellulose and wood. In agreement with previously observed trends (Antal and Mok, 1990), an increase in the heating rate decreases both the char yield and the conversion time. When the high temperature source (at $r = R_T$) is moved closer to the particle surface, t_c changes as a result of two competing processes: the increase in T_p due to the increasing heating rate, and the decrease in temperature due to endothermic reactions. The reduced conversion times imply that it is the first process which dominates in the small R_T/R_p limit. However, the char yields only show mild relative decreases for the smallest R_T values, indicating that the effective pyrolysis temperature is only raised by a relatively *small* amount for the present parameters. Even for the most rapid conversions, the efficiency ratios indicate that diffusion effects cannot be neglected in the accurate simulation of the particle pyrolysis considered here.

An additional interesting result suggested by Fig. 12 concerns the free stream boundary placement. The variation of R_T indirectly gives a measure of the distance from the particle at which the computational boundary must be placed in order to correctly simulate particle pyrolysis within an infinite domain. Numerical simulations of liquid droplet combustion generally require external droplet resolutions greater than 25 times the initial droplet radius in order to eliminate effects due to the boundary placement (see Harstad and Bellan, 1991). Figure 12 indicates that a much smaller domain can be considered in the ease of solid particle pyrolysis. In fact, only very small variations in both char yield and conversion time are observed for values of $R_T > 5R_{p,0}$. The differences between pyrolysis and liquid droplet simulations are due to the nature of the processes. Liquid fuel combustion generally involves initial evaporation followed by second order reaction kinetics with rates which are mixing (diffusion) controlled. Boundary placement near the droplet will significantly increase the mixture fraction of free stream species at the droplet surface. In addition, exothermicity of liquid fuels is generally much larger than the pyrolysis gas phase reactions, resulting in substantial thermal expansion effects relatively far from the droplet. The trends observed for both cellulose and wood particles indicate that the value $R_R = 10R_{p,0}$ is sufficiently large to make boundary placement effects negligible for the final yields and conversion times.

3.2.2 *Effects of the particle size*

It is commercially desirable to pyrolyze large biomass particles as the grinding process necessary to reduce the particle size is overly expensive (DiBlasi, 1993). Kinetic limits arc not necessarily applicable for modeling biomass pyrolysis in reactors. Simmons and Gentry (1986) investigate kinetic limits for pyrolysis control as a function of both $R_{p,0}$ and the heating temperature, Using a mathematical model with prescribed particle surface conditions they estimated that a $200\mu m$ biomass particle is heat transfer limited for temperatures larger than $775K$. However, comparisons with experiments indicated limiting values well below the model predictions. This

discrepancy was attributed to the neglect of the thermal boundary layer outside of the particle in the model. The current work addresses the issue of particle size on pyrolysis yields and kinetic efficiencies for relatively large initial particle sizes and accounts for all inner and outer particle effects.

Figure 13 illustrates the effect of the initial particle size on the final char yields and conversion times. The initial particle diameter is varied in the range $[0.05cm, 2.0cm]$. Both the char yield and t_c are observed to be increasing functions of $R_{p,0}$. However, only relatively small changes in char yield are found for particles larger than $R_{p,0} \approx 0.4cm$. Below this value there is insufficient particle mass for the endothermic reactions to overcome heat diffusion from the surroundings. Therefore, the particle is pyrolyzed at higher effective heating temperatures. For particles larger than this limit, endothermicity maintains an approximately constant effective heating temperature in agreement with the results of Fig. 9. For the given reactor conditions, the optimal particle size for char maximization is approximately $0.4cm$. Larger particles will produce only relatively small increases in char yield, at the expense of substantially longer reactor residence times (minutes-~how-s). The data also reveals that only wood pyrolysis approaches the kinetic control limit within the range of parameters investigated. The conversion efficiencies for the smallest initial particles sizes are 0.004 and 0.42 for cellulose and wood, respectively.

3.2.3 *Effects of the initial porosity*

The initial porosity of the biomass particle can also affect the pyrolysis behavior. Porosity is directly related to the particular biomass specimen under consideration; however, it is not an intrinsic property of the substance. Values of the porosity in hard woods have been reported in the range $0.71 < \varepsilon_0 < 0.85$ by Magnaterra et. *al.* (1992) using both porosimetry and electron scanning microscopy and may be smaller for compactified biomass. Results are presented in Fig. 14 for char yields and conversion times as a function of ε_0 in the range [0.4, 0.9]. This range of values is sufficient to capture the pertinent characteristics of a variety of viable pyrolysis materials, yet is sufficiently large to remain within the bounds of the assumptions used in the model derivation. The total mass of each particle remains constant due to the prescribed values for the initial partial densities of cellulose and wood (Table 2). Figure 14 reveals several interesting influences of ε_0. The char yields for both cellulose and wood remain nearly constant over the entire range of considered porosities due in part to the fixed initial particle mass. On the other hand, t_c shows an increasing trend with initial porosity for both cellulose and wood. Therefore, the effective heating rates of the particles are being decreased with increasing ε_0. This can be explained in terms of the thermal conduction model employed in the internal energy equation. The effective conductivity λ_{eff} is modeled in terms of a *parallel* conduction model corresponding to volume averaging over the respective solid and gas phase conductivities. Tables 2 and 3 show that the conductivity for the solids is in general an order of magnitude larger than that of the gases. Therefore, the *parallel* model results in relatively smaller effective heat

diffusion into the particle for increasing ε_0. A mass averaged conduction model would be expected to show very little effect of ε_0 on t_c. Further experimental results are needed in order to ascertain which type of conduction model is more realistic. Experimentally derived plots of the char yield and t_c versus ε may indicate the correct modeling approach for the effective conductivity.

3.2.4 *Effects of the initial particle temperature*

Onc method of testing the reliability of results in experiments is to pre-treat the biomass before analysis. Varhegyi and Antal (1989) employed thermal prc-treatment in addition to investigating the effects of catalysts ($NaCl$, $FeSO_4$, $ZnCl_2$) on Avicel cellulose pyrolysis. Although the presence of the catal ysts altered the reaction kinetics, pre-treatment of the pure specimen at $535K$ for 1 hour did not produce significant changes in the observed evolutions. Other experiments have addressed the issue of ambient pressure and its effect on the pyrolysis. For example, Richard and Antal (1992) were. able to increase char yields from 6% to 410/0 by raising the pressure from 0.1 MPa to 1.0MPa for the pyrolysis of cellulose in a packed bed reactor. The present CC11U1OSC and wood kinetics schemes do not allow for the investigation of catalyst, thermal prc-treatment duration or pressure effects. However, the value of $T_{p,0}$ can be expected to affect t_c, and possibly the char yield. Figure 15 illustrates these effects by varying $T_{p,0}$ in the range $300K \leq T_{p,0} \leq 600K$. It is evident that $T_{p,0}$ dots not significantly affect the effective pyrolysis temperature as both CC11U1OSC and wood char yields remain nearly constant. Conversion times arc decreased with increasing $T_{p,0}$, as expected. However, the time required to raise the particle temperature from $300K$ to $600K$, *as* estimated from the difference in conversion times, is approximately 100s. This value is significantly less than the total conversion time and gives further evidence that it is the endothermicity of the solid phase reactions which primarily governs conversion times and, therefore, on effective heating rates.

3.3 *Comparison with experiments*

The simulations presented in this work have not been conducted with the intent of representing either the conditions *or* parameters of specific experiments. However, comparisons with past laboratory results arc useful in interpreting the validity of the particle model, as well as the cellulose and the wood kinetics schemes. The minimum requirement from a model or kinetic scheme is that it should predict the total char (and therefore the vapor) yields and also the required time for complete conversion. To the author's knowledge, there arc no *experiments* with measured yields and/or conversion times for "large" isolated cellulose or wood particle pyrolysis. This is because it is advantageous to consider very fine particle. sizes (kinetically controlled pyrolysis) when measuring reaction rate parameters. Nevertheless, by comparing simulations with available data for a variety of conditions and materials, it is possible to qualitatively evaluate both the particle model and kinetics schemes. The two kinetics schemes addressed in this work place limits on the total possible char yields and conversion times (sec

Fig.7). Limiting the discussion to T_R in the range $[550K, 1100K]$ (corresponding to total pyrolysis time scales less than $\sim 10^6 s$), then the possible available char yield must be less than $\approx$ 0.2 for the cellulose scheme, whereas the wood scheme limits char yields to a range of approximately (0.27, 0.32). Any experimental evidence for char yields outside of these ranges would indicate an inconsistency in the modeled pyrolysis kinetics.

In Fig. 16 comparisons are made for the total char yield as a function of T_R for the baseline case cellulose and wood particles with the results of seven experiments. Two different sets of measurements conducted with pure CC11U1OSC arc included. Shafizadeh *et. al. (1979)* performed experiments using cellulose powder in a vacuum tube furnace at relatively low temperatures. The very fine powder sizes in addition to the low heating temperatures suggests that the pyrolysis is nearly completely kinetically controlled. In agreement with this hypothesis, the experimental data compare very well with the kinetic limits of the present mode]. Cellulose pyrolysis in both fluid bed and entrained flow reactors was studied for a larger temperature range and particle size ($R_{p,0} \approx 50 \mu m$) by Scott et. al. (1988). As may be expected, the larger particle size shows slightly more char yield than dots the vacuum pyrolyzed powder. The data reveal that the slightly larger particles employed by Scott *et.* al. still pyrolyze near the kinetic limit. The much larger particle size ($R_{p,0} = 5mm$) considered in our simulations is dominated by diffusion limitations and, as such, shows larger char yields than either experiment. However, the smallest cellulose particle considered in the current work has $R_{p,0} = 0.25mm$ and was pyrolyzed at $T_R = 900K$ (see Fig. 13). In this case, the final char yield is approximately 0.02; comparable to the data of Scott ct. al. (1988). Both sets ofexperirnentrd cellulose char yields are *consistent* with the limits imposed by the model kinetics scheme (< 0.2). The cellulose kinetics scheme is thus considered to be in good agreement with experiments, and the numerical particle model shows the correct qualitative behavior for diffusion dominated pyrolysis.

Experimental data from wood pyrolysis show that the wood kinetics scheme is inadequate. Figure 16 includes four sets of experimentally obtained data for wood pyrolysis. Thurner and Mann (1981) measured char yields from the pyrolysis of Oak sawdust ($R_{p,0} \sim 1\ mm$), over a relatively low temperature range, using a furnace reactor at atmospheric pressure. Their results suggest a nearly constant char yield of approximately 0.3 over the temperature range $[602K, 665K]$. Good agreement with both the wood particle model and the kinetic limit is observed (Fig. 16). This is not surprising as the primary reaction constants used in the current model were extracted from the Thurner and Mann measurements. The small over prediction as compared to their data is a result of the secondary char producing reaction (K_8) which was not originally included in their kinetics scheme. The remaining wood pyrolysis data are for Poplar wood and Olive husk measured in a semi-batch moving bed reactor by Maschio (1992), and for Eastern Red Maple pyrolyzed in both a fluid bed and a transport reactor by Scott et. al. (1 988). All of these experiments used relatively small particle sizes in order to remain near the kinetic control limits, Relatively good agreement is found between the experiments and the model for only the

lowest temperatures considered (near kinetic control). However, all of the experiments display a much sharper reduction in char yield with increasing reactor temperatures than either the particle model or the kinetic scheme is capable of producing. Analysis of Fig.7 indicates that the wood kinetics scheme is not capable of reproducing the lower experimental data for any reactor temperature. These results reveal a major flaw in the present wood pyrolysis scheme in predicting char yields.

Although not included in the data of Fig. 16, the present model results ean be used to make a qualitative assessment of the modified wood kinetics scheme used in both Di Blasi (1993a) (paper 1) and Di Blasi (1992) (paper 11). The modified wood scheme is essentially the same as the present wood kinetics scheme except that the original primary reaction frequency constants presented in Thurner and Mann (1981) were modified by the author (apparently increased by a factor of 3600) (Di Blasi, 1996a). Both papers I and II provide tabular data for char yields at a time when 10% of the original particle mass remains, and with $T_R \approx$ 1100K. In both cases, nearly constant char yields are reported with very little deviations over a relatively wide range of parameters. The respective mean char yields are approximately 0.41 and 0.49 for papers I and H. The discrepancy between char yields obtained with apparently the same reaction scheme has not *been* explained. In addition, the final yields are even higher when the remaining particle mass is consumed. Since a comparison with Fig. 16 shows that these char yields are exceedingly high, it seems that the modified scheme of Di Blasi is of questionable merit.

Quantitative comparisons with experimentally measured conversion times are difficult to make. This is particularly true since such reported data arc usually in terms of particle residence times in the reactor. Even when complete pyrolysis conversion is achieved, the final times are not generally tabulated. However, some data exist which show that the present model is in approximate agreement with experiments. Figure 13 illustrates that the smallest cellulose particle ($R_{p,0} = 0.25mm$) converts completely in 1.6s at a reactor temperature of $T_R = 900K$. This value compares favorably to the 0.7s residence time for an Avicell cellulose particle of initial radius of $R_{p,0} \approx 0.3mm$ in a $973K$ reactor measured by Scott *et. al.* (1988). Oak sawdust pyrolysis at temperatures $627K \leq T_R \leq 665K$ occurs on total reaction time scales bet ween 23 and 31 minutes according to Thurner and Mann (198 1). Again, these values arc similar to the present simulation results as depicted in Fig.6 for slightly larger particles ($\approx$ 2000s). These comparisons suggest that the present particle model is able to reproduce experimental conversion times for both cellulose and wood particles with a reasonable degree of accuracy.

4 CONCLUSIONS

A mathematical model is presented which is capable of modeling both the temporal and the spatial evolutions of porous solid particle reactions for which volumetric reaction rate kinetics are known a *priori.* The model is derived for conditions in which both the porosity and the permeability arc assumed large enough to allow for

continuous gas phase flow within the particle, and is valid in both the interior and the exterior particle regions. Although the equations arc relatively intensive computationally, they provide an accurate representation of particle reactions which may be used to evaluate various kinetics schemes for detailed comparisons with experiments and previous models.

The mathematical model is used to simulate the pyrolysis of spherical biomass particles in initially quiescent super-heated steam environments by considering previously published kinetics schemes for both cellulose and generic wood reactions. As many as five competing reactions arc employed, including complete property variations, thermal and mass transport, and both endothermic and exothermic heats of reaction. Numerical solutions to the modeled equations are used to illustrate the effects of the reactor temperature, heating rate, porosity, initial particle size and initial particle temperature on both char yields and conversion times. Solutions for "baseline case" particles reveal that the modeled equations are capable of reproducing the qualitative evolutions of the pyrolysis process as observed in past experiments and models.

In general, the variation of any parameter which produces an increase in the effective pyrolysis temperature will reduce both the total char yields and the conversion times for both cellulose and wood particles. Such parameter changes include; 1) increasing the reactor temperature, 2) increasing the heating rate, or 3) decreasing the initial particle size. However, practical limits on maximum effective pyrolysis temperatures are imposed by the relative endothermicity of the interior pyrolysis reactions (as related to the particle mass), and also to a lesser extent by thermal diffusion and heat capacity effects. As the particle is heated from its initial value, three stages of evolution are observed. First, an initial rapid heating during which only negligible reactions occur. This is followed by a period of primary pyrolysis which occurs at relatively constant effective pyrolysis temperatures determined by the relative endothcrmicity. The final regime is reached when the particle mass has been reduced sufficiently to allow the inward thermal diffusion to overcome endothermic heat absorption. The remaining particle mass is then rapidly heated until pyrolysis completion occurs, generally at temperatures less than the reactor temperature. Both the mean particle temperature and the heating rate are observed to be almost identical when time is normalized by the final conversion time. In all cases considered, the *three* pyrolysis regimes correspond to approximately 20%, 60% and 20% of the total conversion time, respectively.

The simulated results show that models which neglect the exterior particle thermal boundary layer can substantially over predict both the pyrolysis rate and the experimentally attainable tar yields. Variations of either the initial porosity or the initial particle temperature primarily affect the conversion time, whereas only relatively minor deviations in the total char yields are observed. An increase in the conversion time with increasing porositics is attributed to the *parallel* thermal conduction model employed for the multi-phase heat transfer within the particle. This trend needs further validation through future experiments. In almost all of the particle simulations

considered, the kinetically controlled assumption proved to be invalid,

A qualitative comparison with experimental results from several investigations is provided. These comparisons indicate that the CCI1U1OSC kinetics scheme provides a relatively accurate prediction of char yields and conversion times over a large range of reactor temperatures. The wood pyrolysis kinetics display fair agreement with experiments for very low reactor temperatures. However, at higher reactor temperatures the wood kinetics scheme substantially over predicts the char yields and is inconsistent with the experimental measurements. It is suggested that significant improvements be made to the wood pyrolysis kinetics scheme before any practical predictions arc attempted. Although the experiment.al data were performed for very small particle sizes in order to exhibit kinetically controlled rates, comparisons with the present particle model have indicated a good qualitative agreement for diffusion limiting particle dynamics. Future work will be aimed at expanding the model in order to portray a variety of reactor conditions, including turbulent diffusion, wall effects, and free stream convection. In addition, a kinetics scheme capable of reproducing experimental wood pyrolysis results is presently under investigation.

ACKNOWLEDGMENTS

This research was conducted at the Jet Propulsion Laboratory (JPL) and sponsored by the U.S. Department of Energy (DOE), with Mr. Neil Rossmeissl (DOE Headquarters) and Mr. D. Hooker (DOE Golden Center) serving as contract monitors, under an agreement with the National Aeronautics and Space Administration, Computational resources are provided by the super computing facility at JPL. The authors wish to thank Mr. Jim Diebold and Dr. Estaban Chornet of the National Renewable Energy Laboratory for helpful discussions, and also Dr. Kenneth Harstad of JPL for advice on the numerical method.

REFERENCES

Antal, M. J. and Mok, W. S. L. Review of methods for improving the yield of charcoal from biomass. *Energy and Fuels*, 4(3):22 *1–225, 1990.*

Antal, M. J. and Varhegyi, G. Cellulose pyrolysis kinetics: The current state of knowledge. *Ind. Eng. Chem. Res., 34(3)*:703–7 *17, 1995.*

Bear, J. *Dynamics of Fluids in Porous Media.* American Elsevier, Ney York, New York, 1972.

Bellan, J. and Cuffel, R. A theory of nondilute spray evaporation based upon multiple drop interactions. Comb. *and Flame*, *51:55-67,* 1983.

Bhatia, S. K. and Perlmutter, D. D. A random pore model for fluid-solid reactions: I. Isothermal, kinetic control. *AIChE Journal,* 26(3):379–386, *1980.*

Bhatia, S. K, and Perlmutter, D. D. A random pore mode] for fluid-solid reactions: 11. Diffusion and transport effects. *AIChE Journal,* 27(2):247–254, 1981.

Bilbao, R., Millera, A. and Murillo, M. B. Heat transfer and weight loss in the thermal decomposition of large wood particles. In A. V. Bridgwater, editor, *Advances in Thermochemical Biomass Conversion,* volume 2, pages 833-845. Blackie Academic and Professional, New York, New York, 1992.

Bradbury, A, G., Sakai, Y. and Shafizadeh, F. A kinetic model for pyrolysis of cellulose. *J. App. Polymer Sci.*, 23:3271–3280, 1979.

Caram, H. S. and Amundson, N. R. Diffusion and reaction in a stagnant boundary layer about a carbon particle. *Ind. Dng. Chem. Fundamentals, 16:171,* 1977.

Chan, W. R., Kelbon, M. and Krieger-Brockett, B. Correlations of reaction products with process conditions. *Ind. Eng. Chem. Ales.,* 27:2261–2275, 1988.

Di Blasi, C. Modeling of transport phenomena and kinetics of biomass pyrolysis. In A. V. Bridgwater, editor, *Advances in Thermochemical Biomass Conversion,* volume 2, pages 906921. Blackie Academic and Professional, Ncw York, Ncw York, 1992.

Di Blasi, C. Analysis of convection and secondary reaction effects within porous solid fuels undergoing pyrolysis. *Combust. Sci. and Tech., 90:315-340,* 1993a,

Di Blasi, C. Modeling and simulation of combustion processes of charring and non-charring solid fuels. *Prog. Energy Combust. Sci.,* 19:71-104, 1993b.

Di Blasi, C. Numerical simulation of cellulose pyrolysis. *Biomass and Bioenergy*, 7:87–98, *1994.*

Di Blasi, C. Personal communication, Feb. 1996a.

Di Blasi, C. Kinetic and heat transfer control in the slow and flash pyrolysis of solids. *Ind. Eng. Chem. Res.*, 35:37–46, 1996b.

Diebold, J. P. Ablative pyrolysis of macroparticles of biomass. In *Proc. Spec. Workshop Fast Pyrolysis of Biomass*, pages 237–25 1, Copper Mountain, Colorado, Oct. 1980. Solar Energy Research Institute.

Diebold, J. P. and Power, A. Engineering aspects of the vortex pyrolysis reactor to produce primary pyrolysis oil vapors for usc in resins and adhesives. In A. V. Bridgwater and J. L. Kuester, editors, *Research in Thermochemical Biomass Conversion,* pages 609-628. Elsevier Applied Science, Ncw York, New York, 1988.

Gavalas, G. R. A random capillary model with application to char gasification at chemically controlled rates. *AIChE Journal,* 26(4):577--585, *1980.*

Gavalas, G. R. Analysis of char combustion including the effect of pore enlargement. *Comb Sci. and Technol.*, 24:197–210, *1981.*

Harstad, K. and Bellan, J. A model of the evaporation of binary-fuel clusters of drops. *Atom. and Sprays, 1:367-388, 1991.*

Kothari, V. and Antal, M. J. Numerical studies of the flash pyrolysis of cellulose. *Fuel*, 64:1487--1494, 1985.

Lede,J., Panagopoulos, J., Li, H. Z. and Villermaux, J. Fast pyrolysis of wood: Direct measurement and study of ablation rate. *Fuel*, 64:15 14–1520, 1985.

Lim, K. S., Zhu, J. X. and Grace, J. R. Hydrodynamics of gas-solid fluidization. *Fuel*, 21(Suppl.):141-193, 1995.

Loewenberg, M., Bellan, J. and Gavalas, G. R. A simplified description of char combustion. *Chem. Eng. Comm.*, 58:89–103, 1987.

Magnaterra, M., Fusco, J. R., Ochoa, J. and Cukierman, A, L. Kinetic study of the reaction of different hardwood sawdust chars with oxygen. Chemical and structural characterization of the samples. In A. V. Bridgwater, editor, *Advances in Thermochemical Biomass Conversion,* volume 1, pages 116130, Blackie Academic and Professional, Ncw York, New York, 1992.

Maschio, G., Lucchesi, A. and Koufopanos, C. Study of kinetic and transfer phenomena in the pyrolysis of biomass particles. In A. V. Bridgwater, editor, *Advances in thermochemical Biomass Conversion,* volume 2, pages 746-759. Blackie Academic and Professional, New York, New York, 1992.

Mon, E. and Amundson, N. R. Diffusion and reaction in a stagnant boundary layer about a carbon particle . 2. An extension. *Ind. Dng. Chem. Fundamentals*, 17:313, 1978.

Narayan, R. and Antal, M. J. Thermal lag, fusion, and the compensation effect during biomass pyrolysis. *Ind. Eng. Chem. &s., 1996.* submitted.

Reed, T. B., Diebold, J. P. and Desrosiers, R, Perspectives in heat transfer requirements and mechanisms for

fast pyrolysis. In *Proc. Spec. Workshop Fast Pyrolysis of Biomass,* pages 7–20, Copper Mountain, Colorado, Oct. 1980. Solar Energy Research Institute.

Richard, J. P. and Antal, M. J. Thermogravimetric studies of charcoal formation from cellulose at elevated pressures. *in* A. V. Bridgwater, editor, *Advances in Thermochemical Biomass Conversion,* volume 2, pages *784-792.* Blackie Academic and Professional, Ncw York, Ncw York, 1992.

Scott, D. S., Piskorz, J., Bergougnou, M. A., Gr-sham, R. and Overend, R. P. The role of temperature in the fast pyrolysis of cellulose and wood. *Ind. Eng. Chem. Res., 27:8-15,* 1988.

Shafizadch, F., Furneaux, R. H., Cochran, T. G., Scholl, J. P. and Sakai, Y. Production of levoglucosan and glucose from pyrolysis of cellulosic materials. *J. Appl. Polym. Sci.*, 23:3525–3539, *1979.*

Simmons, G. M. and Gentry, M. Particle size limitations due to heat transfer in determining pyrolysis kinetics of biomass. *J. Anal. and Appl. Pyrolysis,* 10:117– 127, 1986.

Sotirchos, S. V. and Amundson, N. R. Diffusion and reaction in a porous char particle and in the surrounding gas 2. Limiting model. *Ind. Dng. Chem. Fundamentals, 23:180,* 1984a.

Sotirchos, S. V. and Amundson, N. R. Diffusion and reaction in a porous char particle and in the surrounding gas. a continuous model. *Ind. Dng. Chem. Fundamentals, 23:191,* 1984b.

Sundaresan, S. and Amundson, N. R. Diffusion and reaction in a stagnant boundary layer about a carbon particle 5. Psuedosteady state structure and parameter sensitivity. *Ind. Dng. Chem. Fundamentals,* 19:344, 1980.

Thurner, F. and Mann, U. Kinetic investigation of wood pyrolysis. *Ind. Eng. Chem. Process Des. Dev.*, 20:482–488, *1981.*

Varhegyi, G. and Antal, M. J. Kinetics of the thermal decomposition of cellulose, hemicellulose, and sugar cane bagasse. *Energy and Fuels,* 3:329–335, 1989.

TABLES

Reaction	A_i [1/s]	E_i [kJ/kmol]	A h_i [kJ/kg]
K,	2.8 x 10^{19}	2.424 x 10^5	o
K_2	1.3 x 10^{10}	**1.505** x 10^5	-418
K3	3.28 X 10^{14}	1.965 X 10^5	-418
K4	4.28 X 10^6	1.08 X 10^5	-t42
K_5	1.43 x **10'**	8.86 x 10^4	-418
K_6	4.13 × 10^6	1,127 x 10^5	-418
K_7	7.38 X 10^5	1.065 X 10^5	-418
K_8	1.0 × 10^5	1,08 X 10^5	+42

Table 1: Reaction parameters.

Species	$(1 - \varepsilon_0)\hat{\rho}$ $[\frac{kg}{m^3}]$	C $[\frac{kJ}{kg}]$	λ $[\frac{kJ}{m \cdot s \cdot K}]$
–cellulose	420	2.3	2.426 x 10^{-4}
active	420	2.3	2.426 x 10^{-4}
char	(420,650)"	1.1	1.046 × 10^{-4}
wood	650	2.3	1.046 x10-4

Table 2: Property values for the solid phase species. The superscript * indicates assumed values.

Species	M_i $[\frac{kg}{kg \cdot mole}]$	C_v $[\frac{kJ}{kg}]$	μ $[\frac{kg}{m \cdot s}]$	λ $[\frac{kJ}{m \cdot s \cdot K}]$	D $[\frac{m^2}{s}]$
H_2O	18.016	2.20	2.9 x 10^{-5}	7.8 x 10^{-5}	1.1 x 10^{-4}
gas	18.016'	1,1	3.0 x 10^{-5}	2.577 x 10^{-5}	1.1 x $10^{-"4}$'
tar	18.016*	2.5	3.0 x 10^{-5}	2.577 x 10^{-5}	1.1 x 10^{-4}*

Table 3: Property values for the gas phase species. The steam values are given for $T' = 800$K and $p = 100kPa$, and the superscript * indicates assumed values.

Reaction	char limit	conversion limit [s]
cellulose	$0.35K_2(K_2 + K_3)^{-1}$	$-\log(0.001)(K_2 + K_3)^{-1}$
	baseline: 6.4 x 10^{-3}	baseline: 5.3 x $10^{-"3}$s
wood	$\{K_7 + K_6 \frac{A_5}{A_4 + A_5}\}(K_5 + K_6 + K_7)^{-1}$	$-\log(0.001)(K_5 + K_6 + K_7)^{-1}$
	baseline: 0.29	baseline: 3.9s

Table 4: Kinetic limits for char yields and conversion times. The baseline values correspond to limits evaluated at $T' = 900K$.

FIGURE CAPTIONS

Figure 1: Reaction schemes: (a) cellulose pyrolysis, (b) wood pyrolysis.

Figure 2: Temporal evolution of the partial char density for the baseline case simulations, (a) CC1IU1OSC, t = 53s, 116s, 187s, 254s, (b) wood, t = 89s, 181s, 268s, 348s.

Figure 3: Temporal evolution of the tar mass fraction for the baseline case simulations, (a) CC11U1OSC, t = 53s, 1 16s, 187s, 254s, (b) wood, t = 89s, 181s, 268s, 348s.

Figure 4: Temporal evolution of the temperature for the baseline case simulations, (a) cellulose, t = 0s, 53s, 116s,187s, 254s, (b) wood, t = 0s, 89s, 181s, 268s, 348s.

Figure 5: Temporal evolution of the gas phase velocity for the baseline case simulations, (a) CCI1U1OSC, t = 53s, 116s, 187s, 254s, (b) wood, t = 89s, 181s, 268s, 348s.

Figure 6: Char yield and conversion time as a function of the reactor temperature for $T_{p,0} = 500K$, $R_T = 5R_{p,0}$, $R_{p,0} = .5mm$ and $\varepsilon_0 = 0.7$.

Figure 7: Kinetic limits for char yield and conversion time as a function of the reactor temperature.

Figure 8: Kinetic efficiency for char yield and conversion time as a function of the reactor temperature for $R_T = 5R_{p,0}$, $R_{p,0} = 5mm$, $\varepsilon_0 = 0.7$ and $T_{p,0} = 500K$.

Figure 9: Mass averaged particle temperature $< T_p >$ as a function of time normalized by t_c for $T_{p,0} = 500K$, $R_T = 5R_{p,0}$, $R_{p,0} = 5mm$ and $\varepsilon_0 = .0.7$; (a) cellulose, (b) wood, The reactor temperature is varied from 700K $\leq T_R \leq$ 1200K in increments of100K.

Figure 10: Temporal derivative ofthc mass averaged particle temperature $< T_p >$ as a function of time normalized by t_c for $T_{p,0} = 500K$, $R_T = 5R_{p,0}$, $R_{p,0} = 5mm$ and $\varepsilon_0 = 0.7$; (a) CCHU1OSC, (b) wood. The reactor temperature is varied from 700K $\leq T_R \leq 1200K$ in increments of $100K$.

Figure 11: Maximum normalized radial position at which the tar fraction has decayed to 5% and the maximum tar fraction as a function of the reactor temperature for both cellulose and wood and for $T_{p,0} = 500K$, $R_T = 5R_{p,0}$,

$R_{p,0} = 5mm$ and $\varepsilon_0 = 0.7$.

Figure 12: Char yield and conversion time as a function of the normalized thermal radius for $T_R = 900K$, $R_{p,0} = 5mm, \varepsilon_0 = 0.7$ and $T_{p,0} = 500K$.

Figure 13: Char yield and conversion time as a function of the initial particle radius for $T_R = 900K, R_T = 5R_{p,0}$, $\varepsilon_0 = 0.7$ and $T_{p,0} = 500K$.

Figure 14: Char yield and conversion time as a function of the initial porosity for $T_R = 900K$, $R_T = 5R_{p,0}$, $R_{p,0} = 5mm$ and $T_{p,0} = 500K$.

Figure 15: Char yield and conversion time as a function of the initial particle temperature for $T_R = 900K$, $R_T = 5R_{p,0}$, $R_{p,0} = 5mm$ and $\varepsilon_0 = 0.7$.

Figure 16: Comparison of final char yields as a function of the reactor temperature with experiments. Both the kinetic limits and simulation results are shown ($R_T = 5R_{p,0}, R_{p,0} = 5mm$, $\varepsilon_0 = 0.7$ and $T_{p,0} = 500$ K): Poplar wood (()) and Olive husk (.) from Maschio et. al. (1992), Avicell CC1IU1OSC (U) and Eastern red maple (■) from Scott ct. al. (1 988), Oak sawdust (A) from Thurner and Mann (1981) and cellulose (◇) from Shafizadeh et. al. (1979).

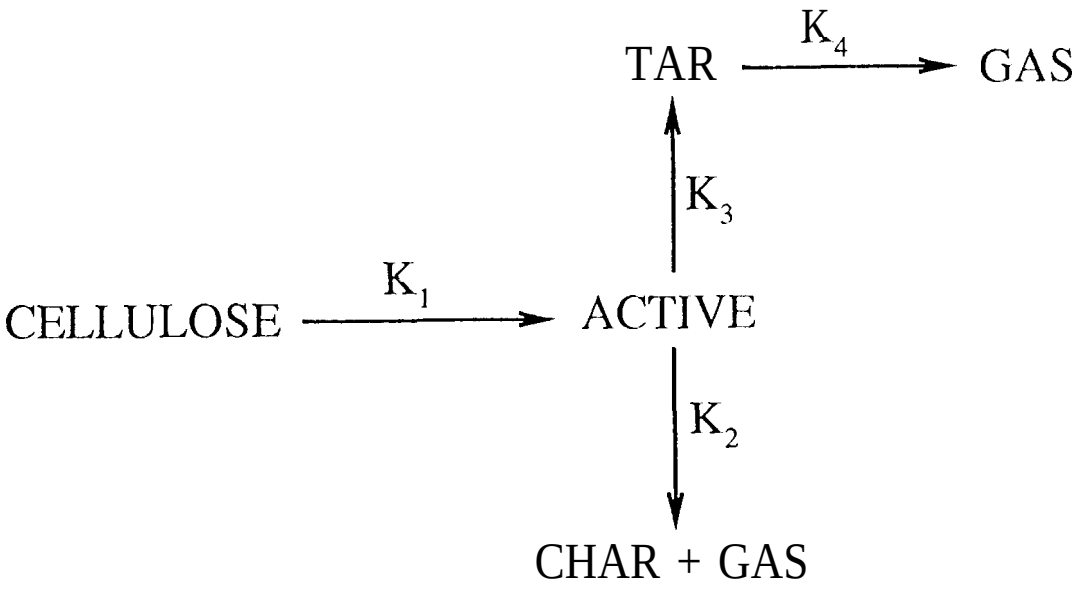

Figure 1a

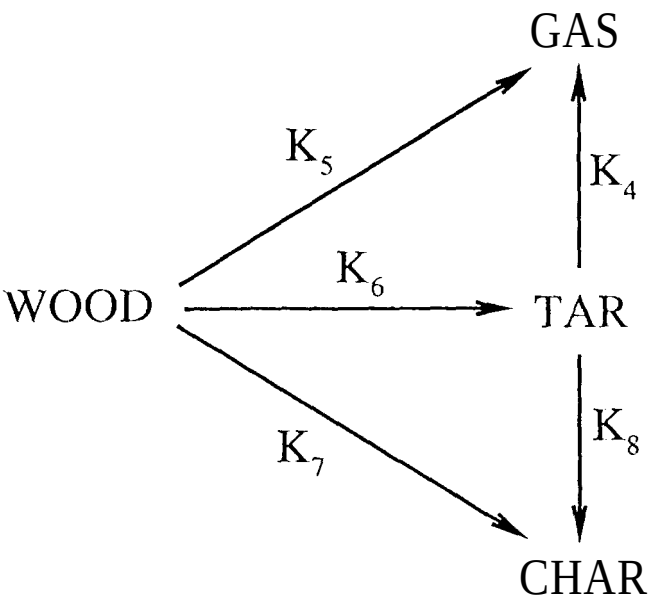

Figure 1b

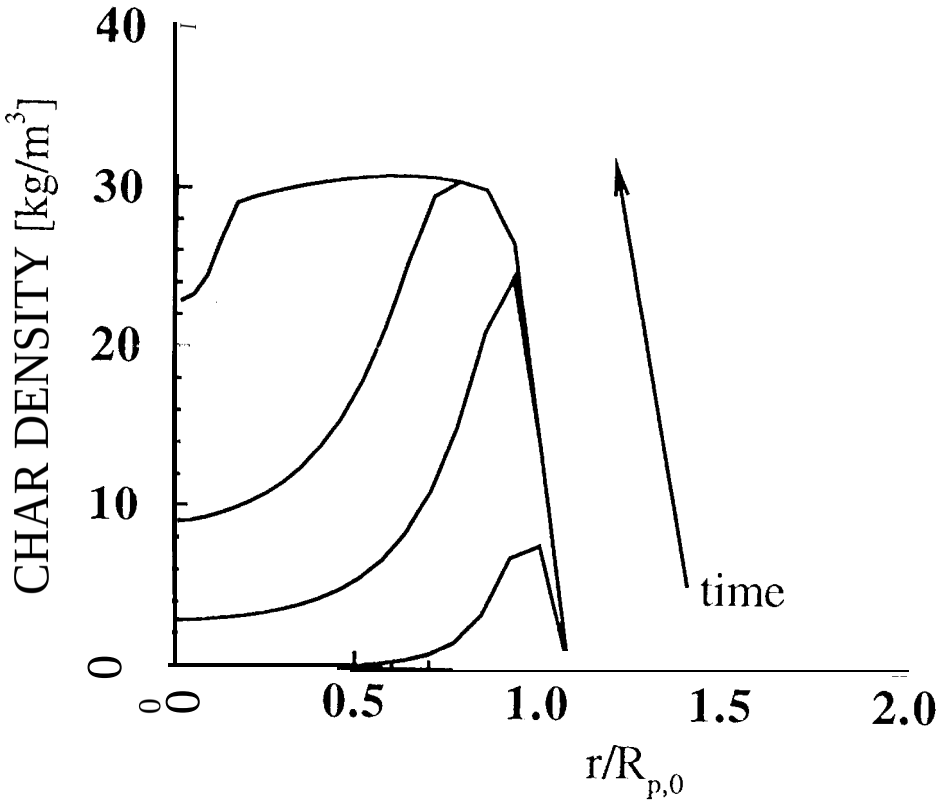

Figure 2a

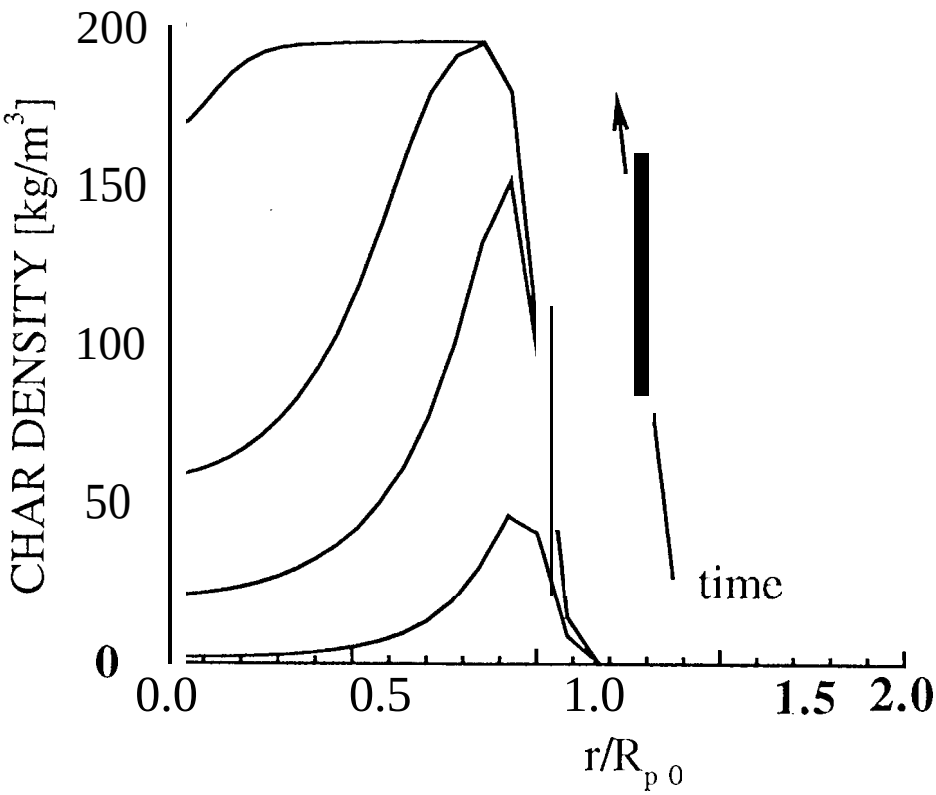

Figure 2b

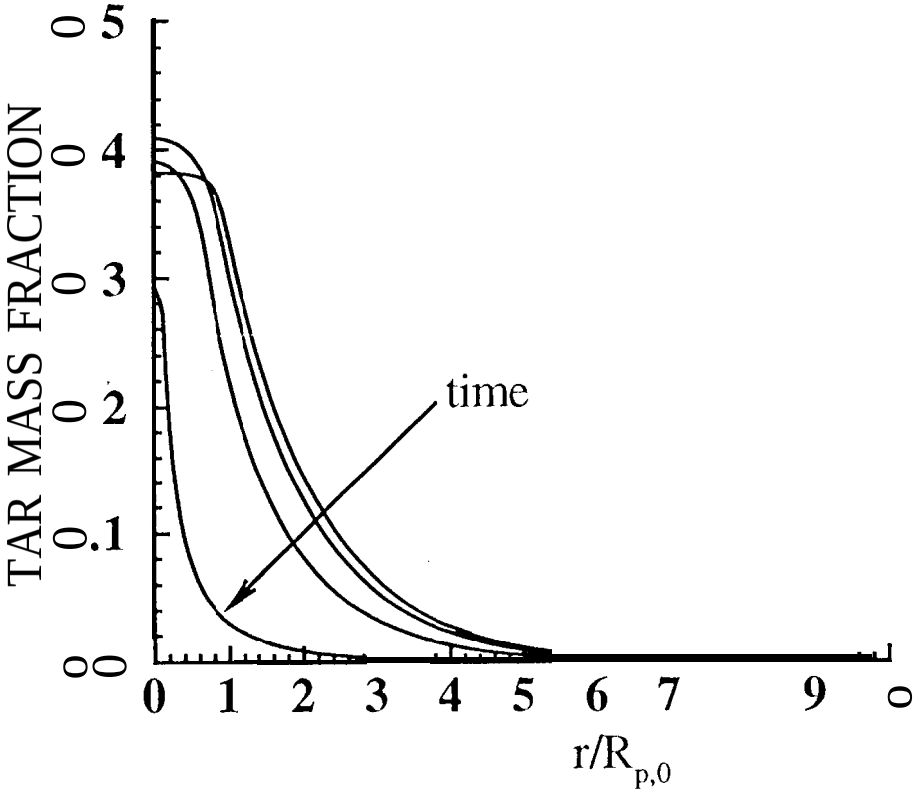

Figure 3a

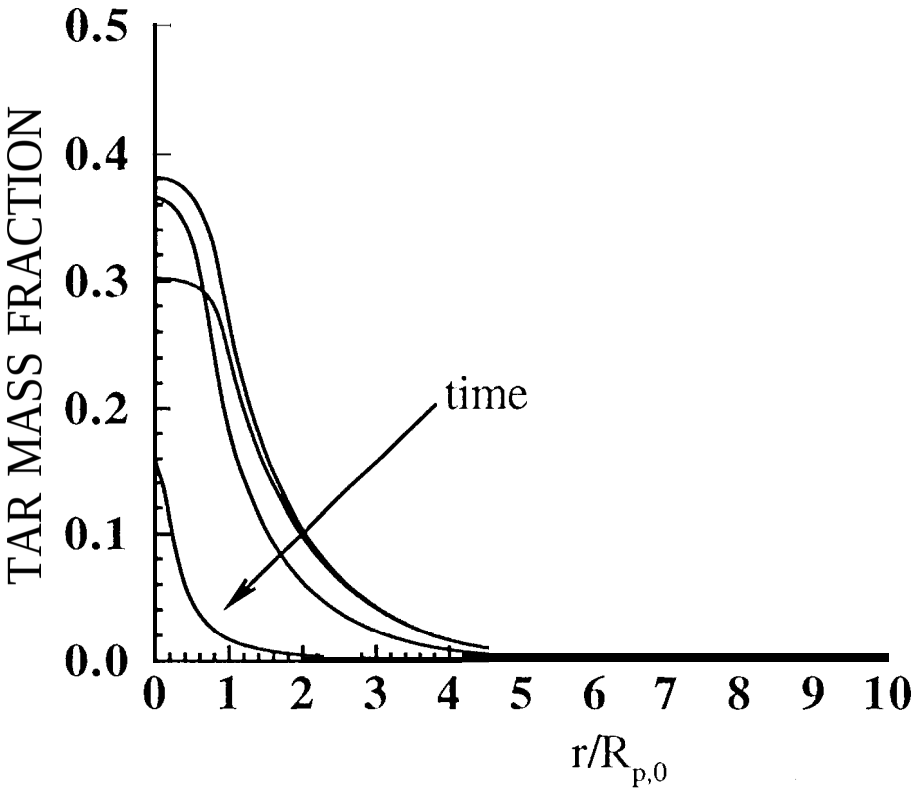

Figure 3b

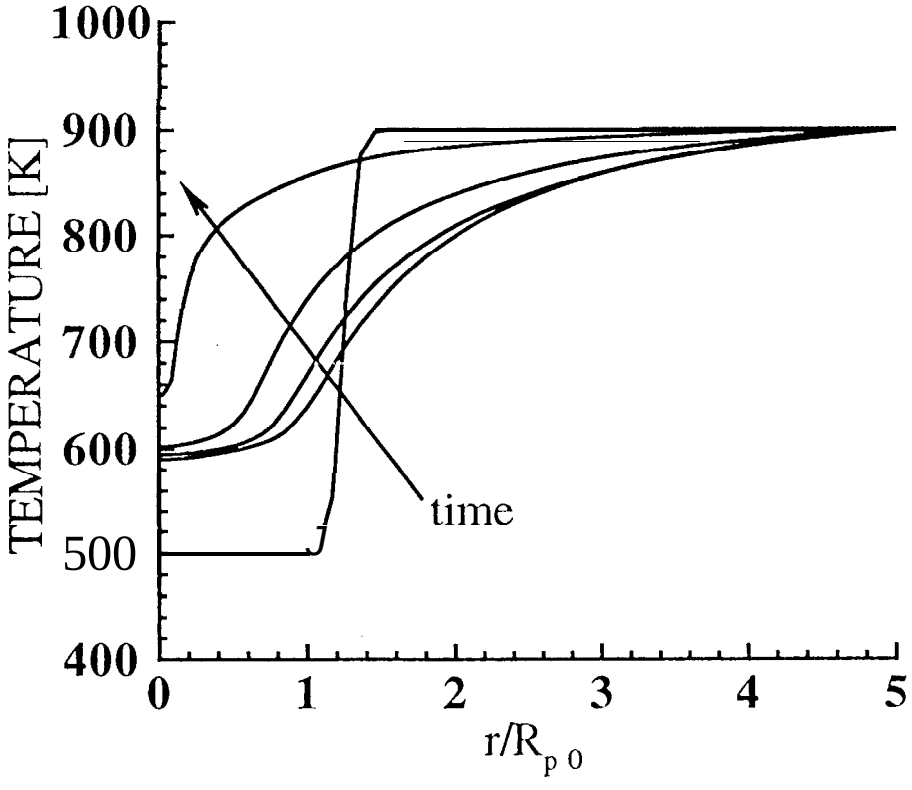

Figure 4a

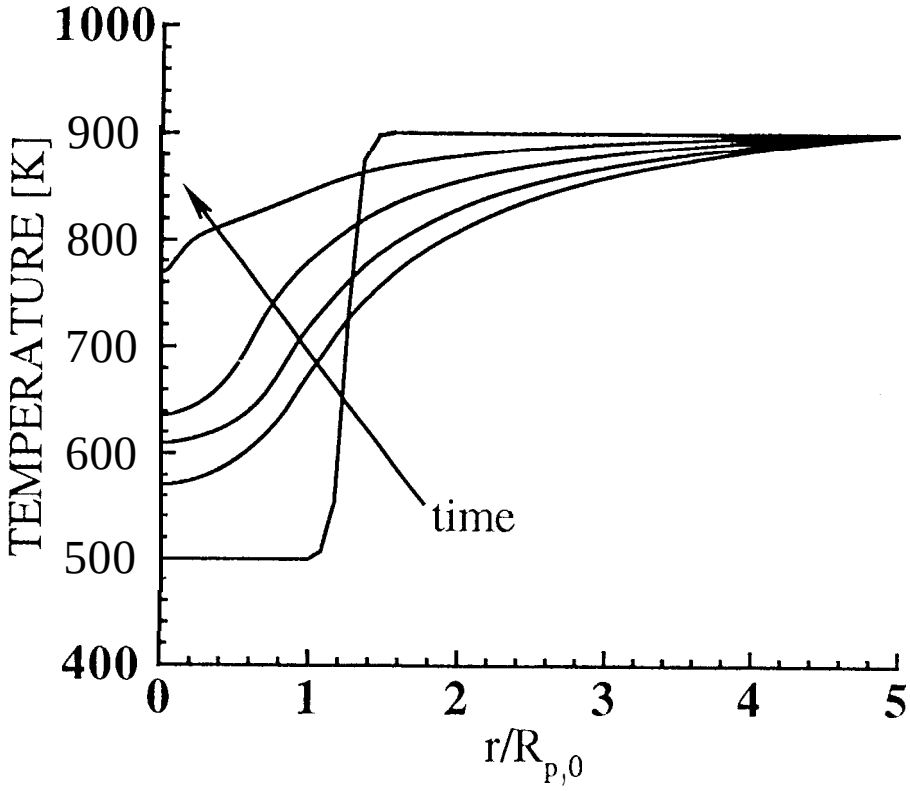

Figure 4b

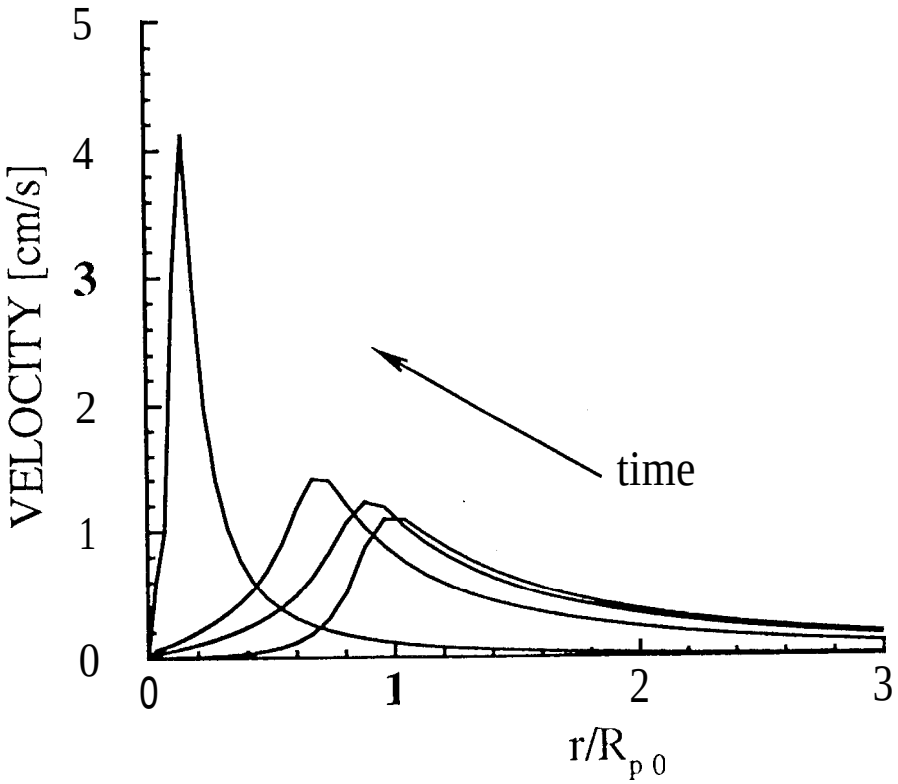

Figure 5a

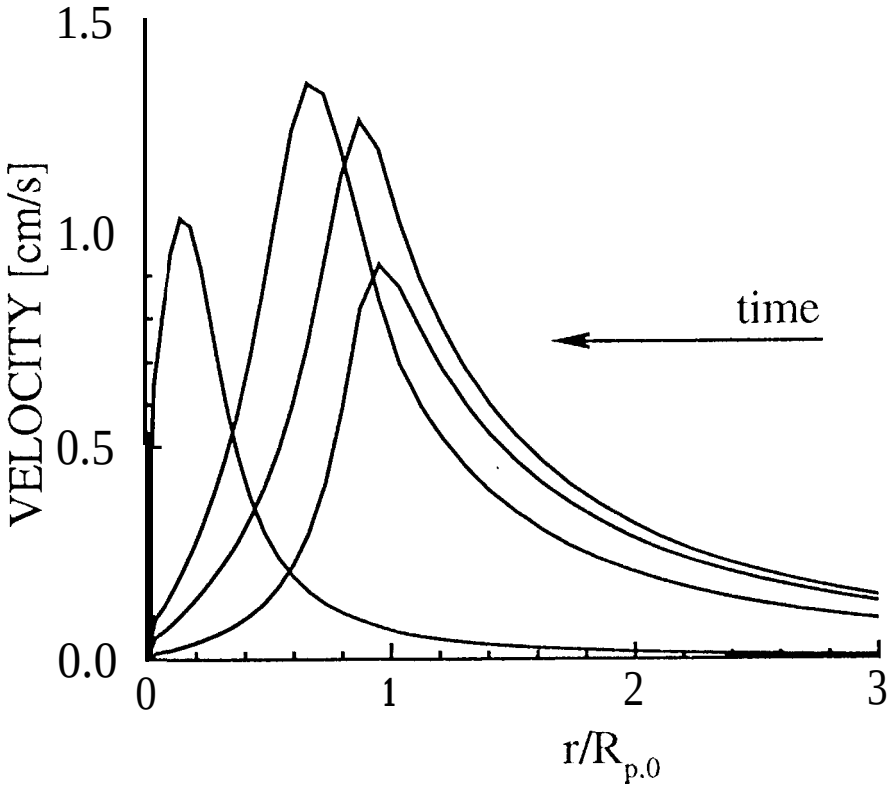

Figure 5b

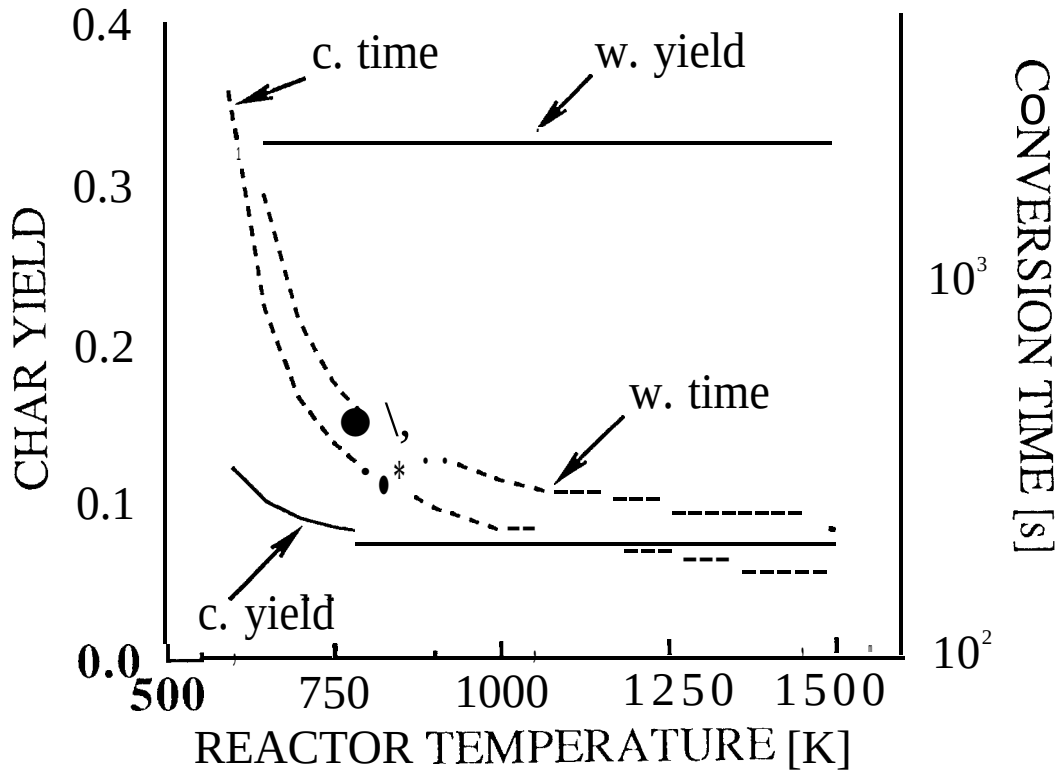
0.4
0.3
0.2
0.1
0.0
CHAR YIELD
c. time
w. yield
w. time
c. yield
10^3
10^2
CONVERSION TIME [s]
500
750
1000
1250
1500
REACTOR TEMPERATURE [K]

Figure 6

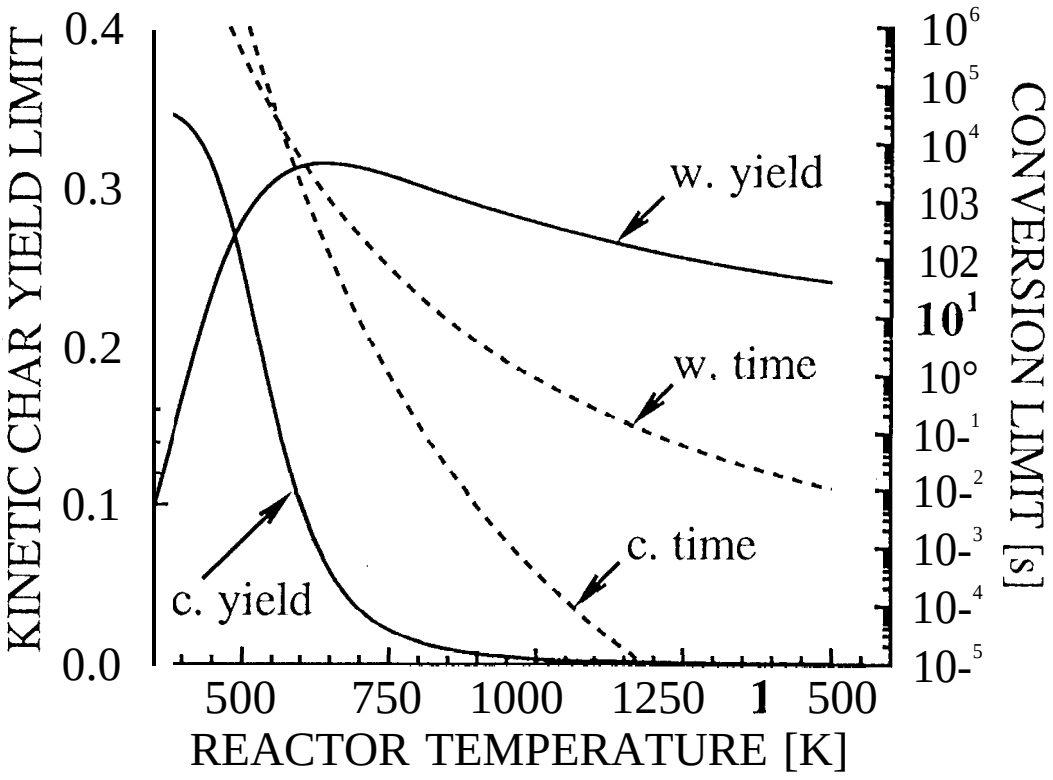
KINETIC CHAR YIELD LIMIT
0.4
0.3
0.2
0.1
0.0
w. yield
w. time
c. time
c. yield
500
750
1000
1250
1 500
REACTOR TEMPERATURE [K]
CONVERSION LIMIT [s]
10^6
10^5
10^4
103
102
10^1
10°
10-^1
10-^2
10-^3
10-^4
10-^5

Figure 7

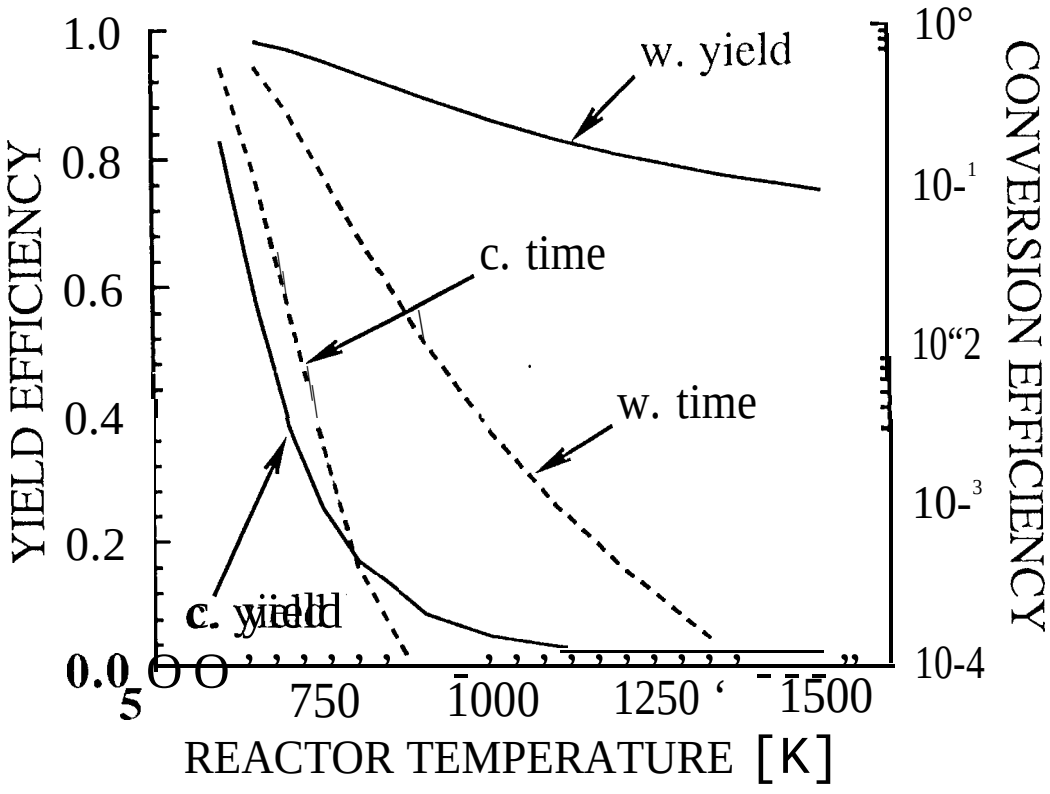
1.0
0.8
0.6
0.4
0.2
0.0
YIELD EFFICIENCY
w. yield
c. time
w. time
c. yield
750
1000
1250
1500
REACTOR TEMPERATURE [K]
10°
10-1
10“2
10-3
10-4
CONVERSION EFFICIENCY

Figure 8

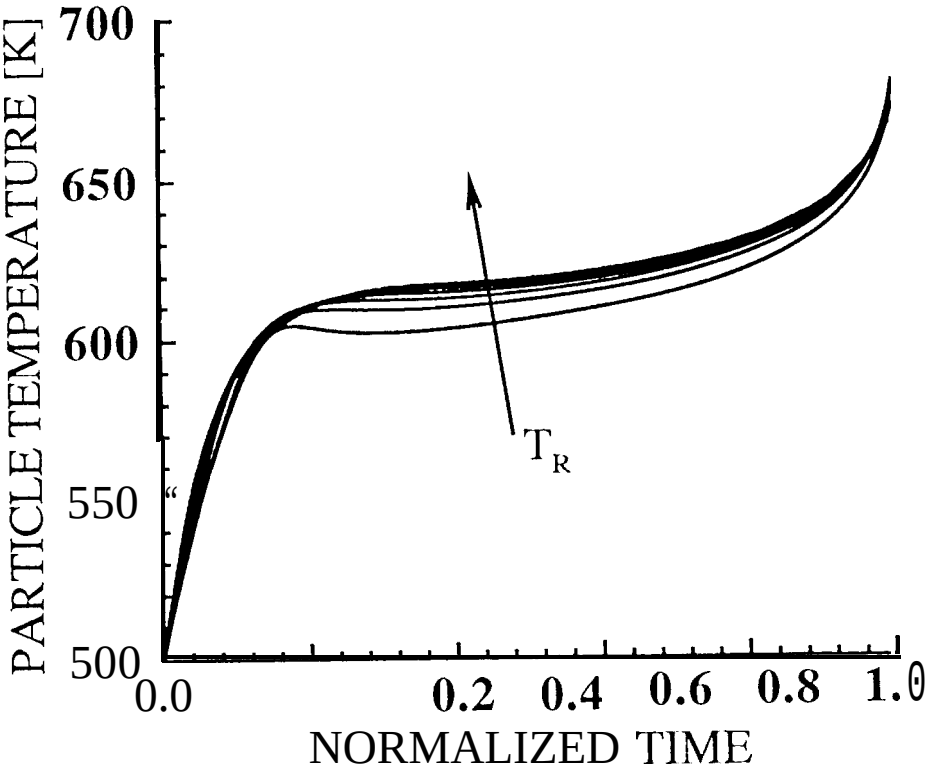
700
650
600
550
500
PARTICLE TEMPERATURE [K]
0.0
0.2
0.4
0.6
0.8
1.0
NORMALIZED TIME
T_R

Figure 9a

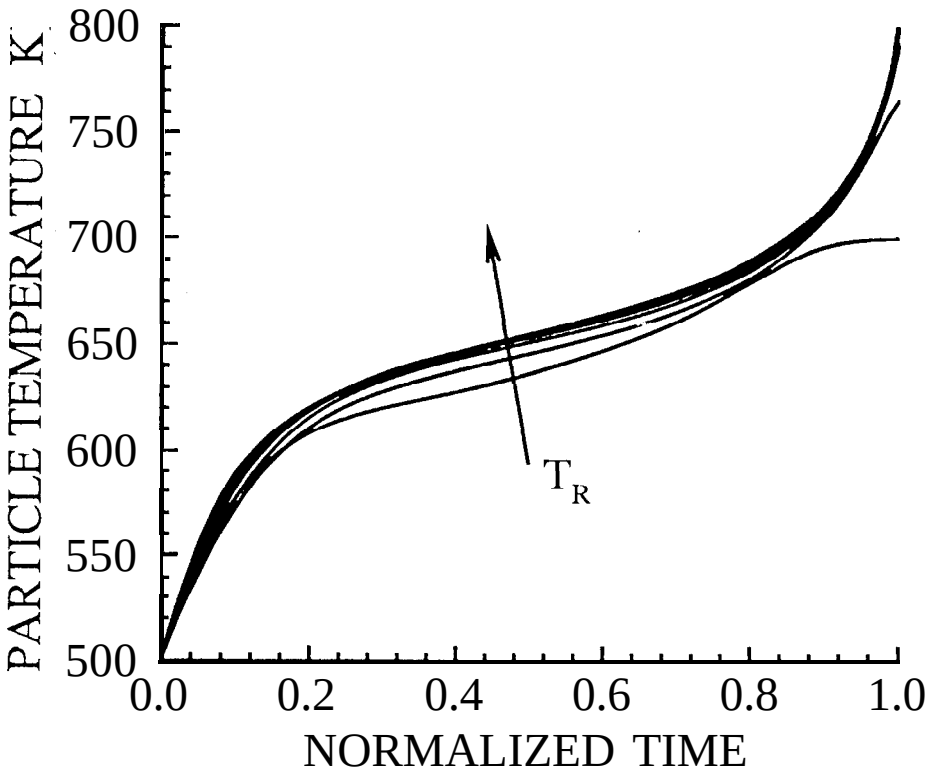
PARTICLE TEMPERATURE K
800
750
700
650
600
550
500
0.0
0.2
0.4
0.6
0.8
1.0
NORMALIZED TIME
T_R

Figure 9b

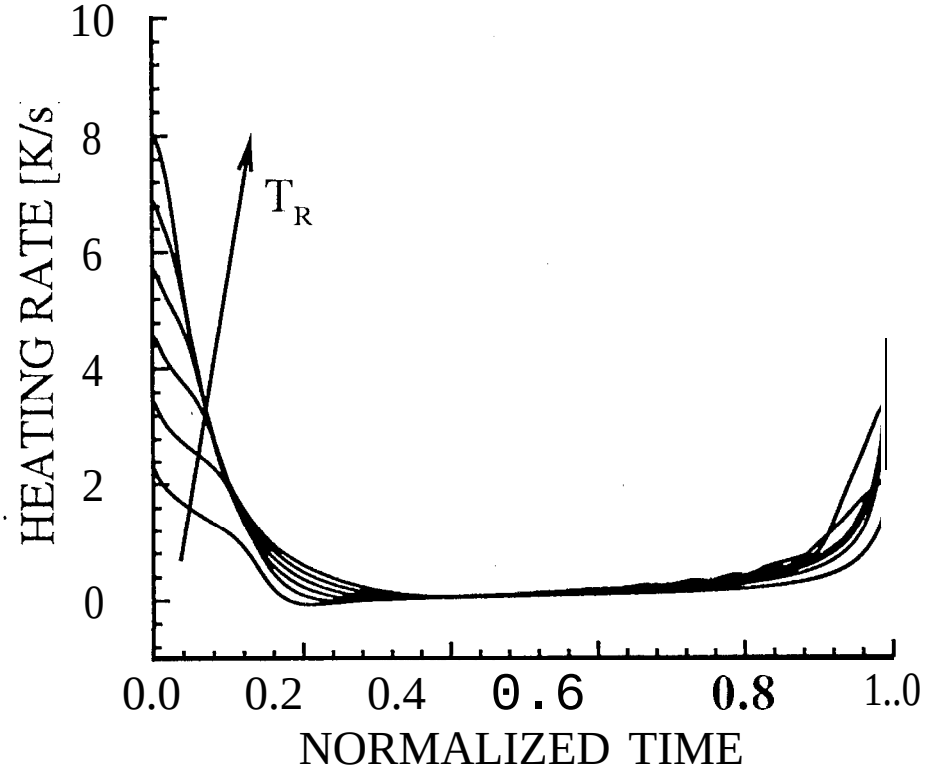

Figure 10a

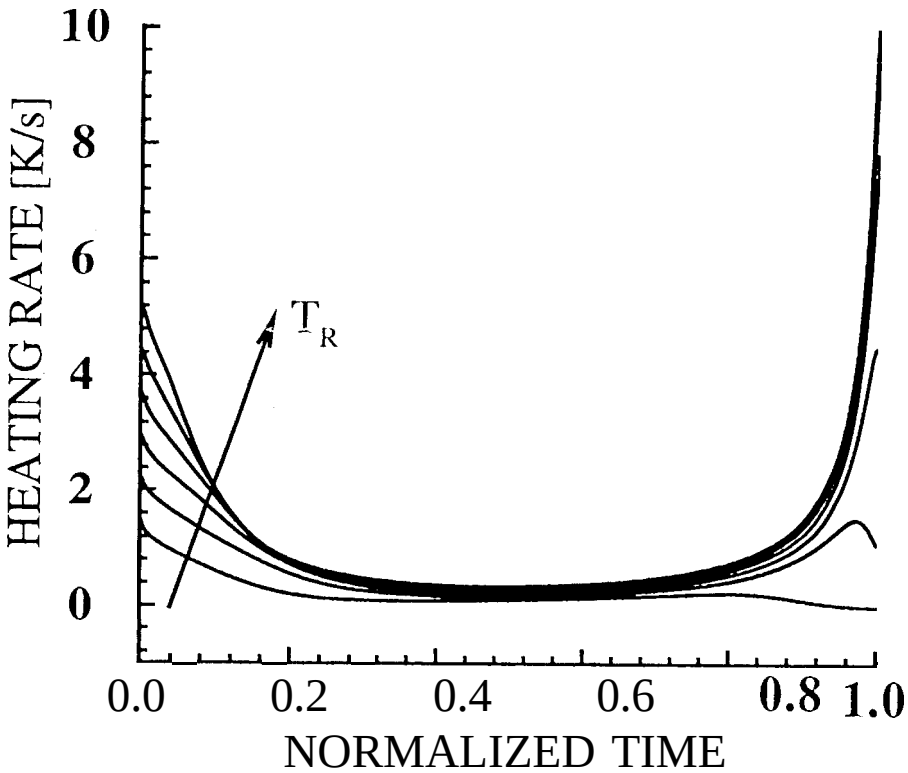

Figure 10b

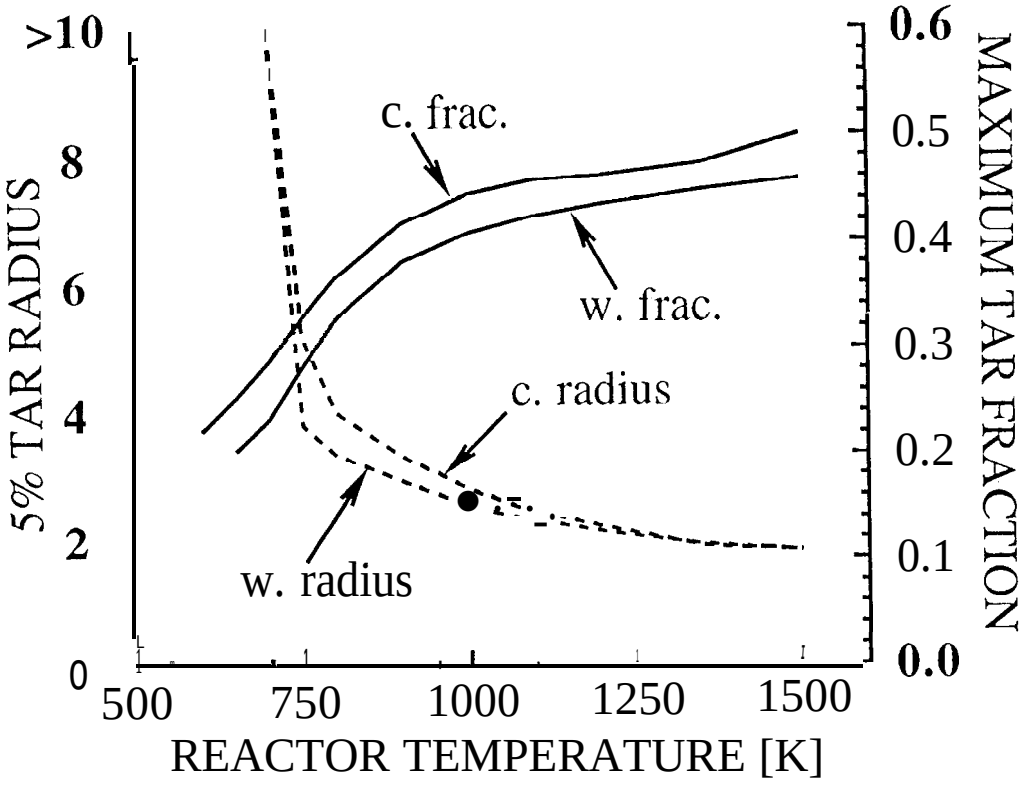
>10
8
6
4
2
0
5% TAR RADIUS
0.6
0.5
0.4
0.3
0.2
0.1
0.0
MAXIMUM TAR FRACTION
c. frac.
w. frac.
c. radius
w. radius
500
750
1000
1250
1500
REACTOR TEMPERATURE [K]

Figure 11

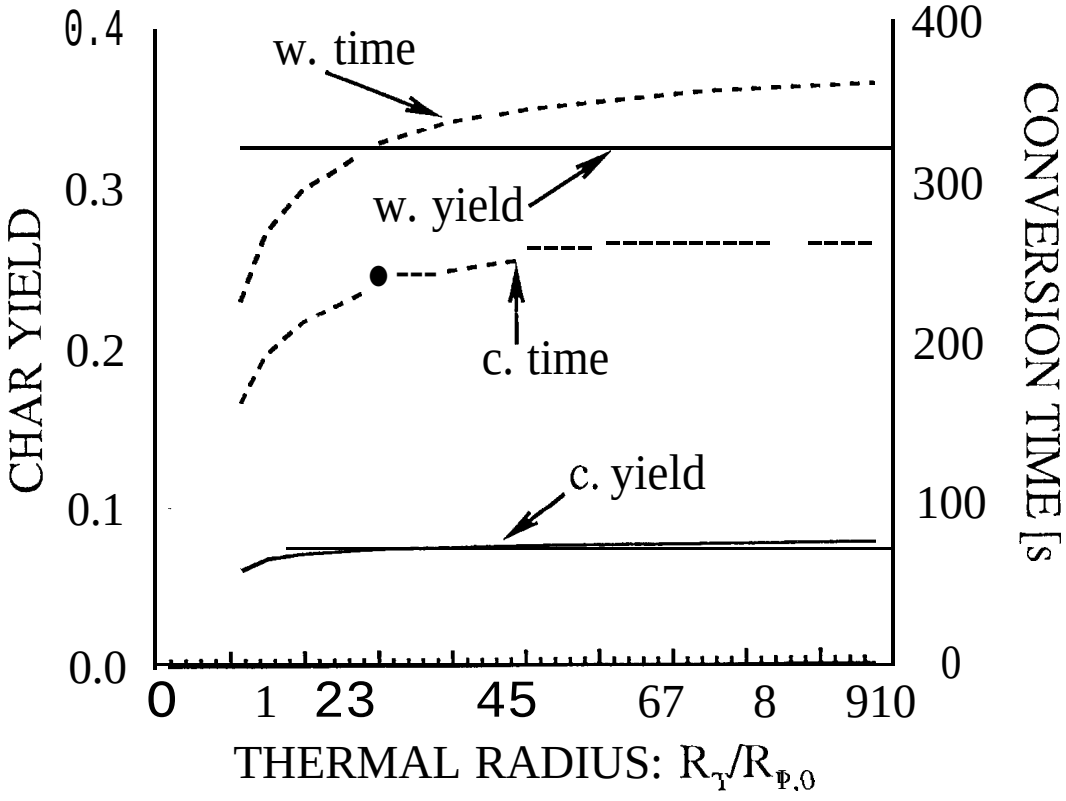
0.4
0.3
0.2
0.1
0.0
CHAR YIELD
400
300
200
100
0
CONVERSION TIME [s
w. time
w. yield
c. time
c. yield
0
1
23
45
67
8
910
THERMAL RADIUS: $R_T/R_{P.0}$

Figure 12

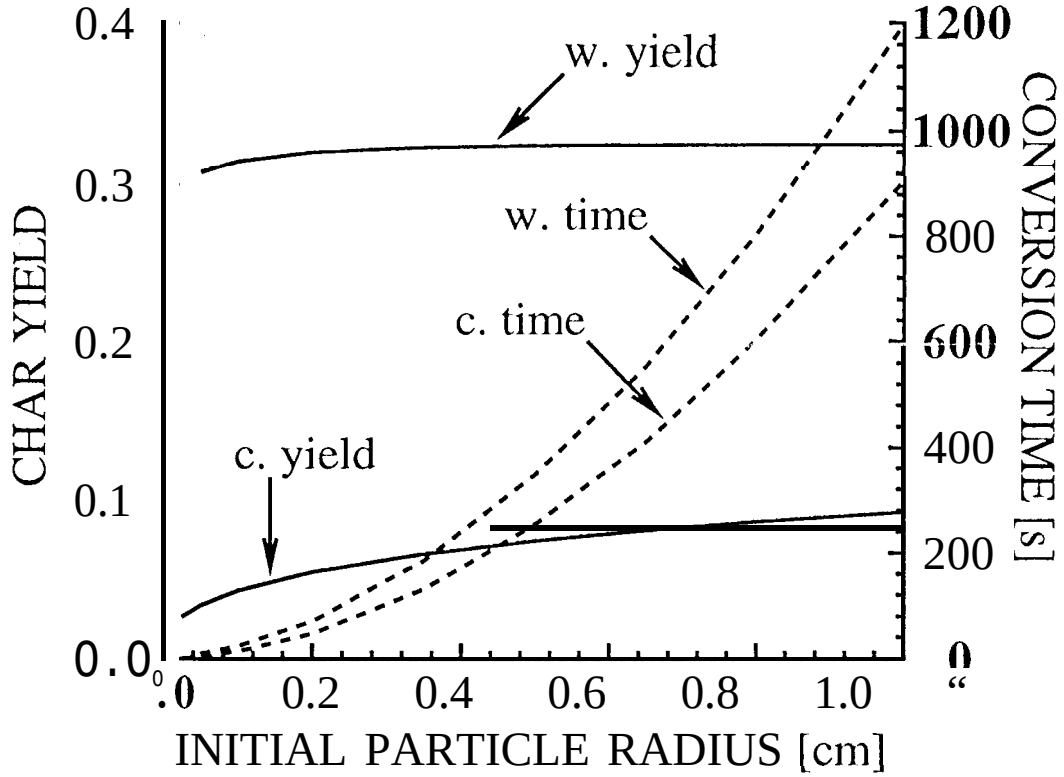
0.4
0.3
0.2
0.1
0.0
CHAR YIELD
w. yield
w. time
c. time
c. yield
1200
1000
800
600
400
200
0
CONVERSION TIME [s]
0.0
0.2
0.4
0.6
0.8
1.0
INITIAL PARTICLE RADIUS [cm]

Figure 13

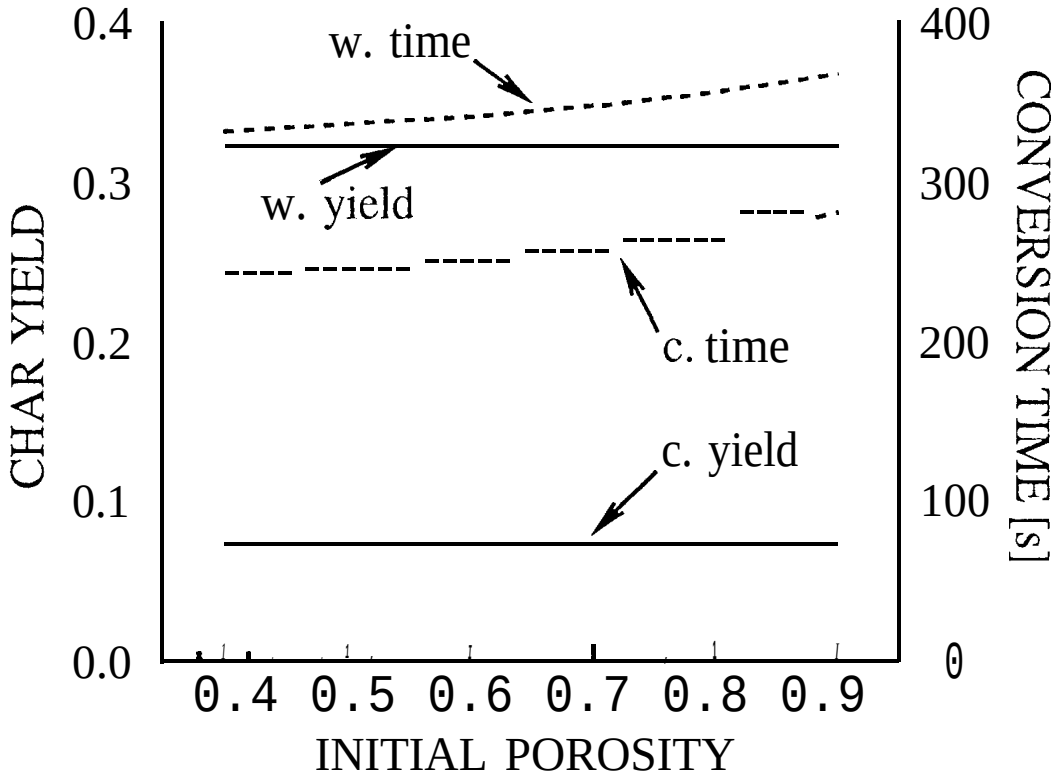
0.4
0.3
0.2
0.1
0.0
CHAR YIELD
w. time
w. yield
c. time
c. yield
400
300
200
100
0
CONVERSION TIME [s]
0.4 0.5 0.6 0.7 0.8 0.9
INITIAL POROSITY

Figure 14

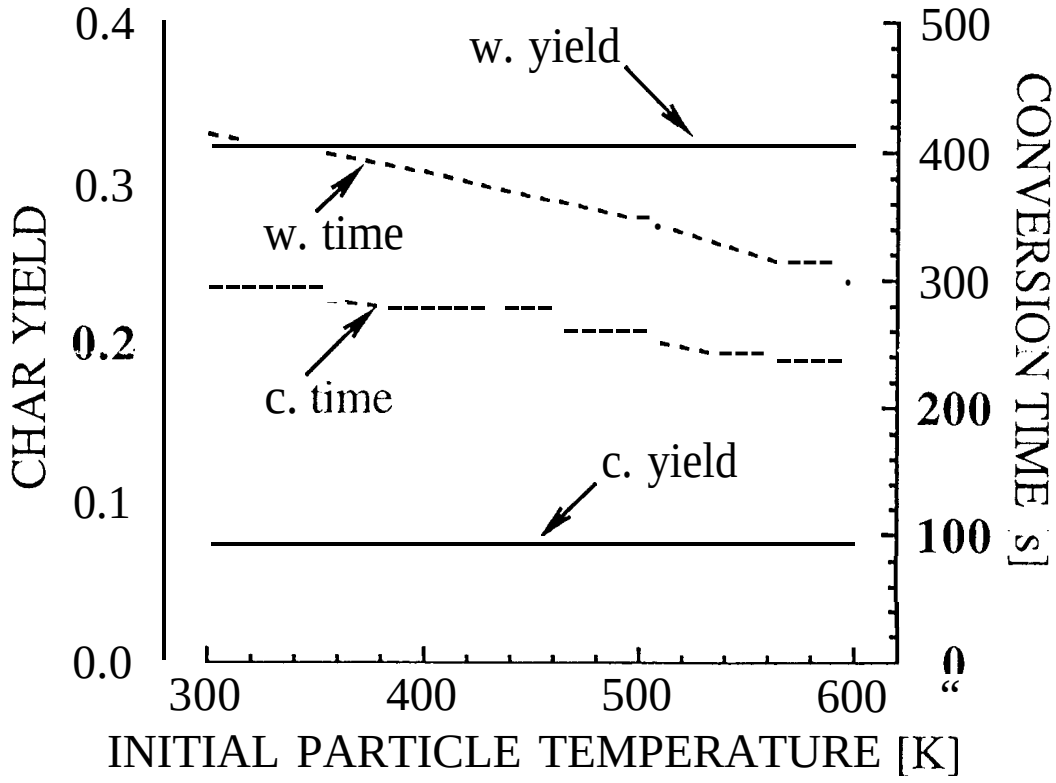
0.4
0.3
0.2
0.1
0.0
CHAR YIELD
w. yield
w. time
c. time
c. yield
500
400
300
200
100
0
CONVERSION TIME s]
300
400
500
600
INITIAL PARTICLE TEMPERATURE [K]

Figure 15

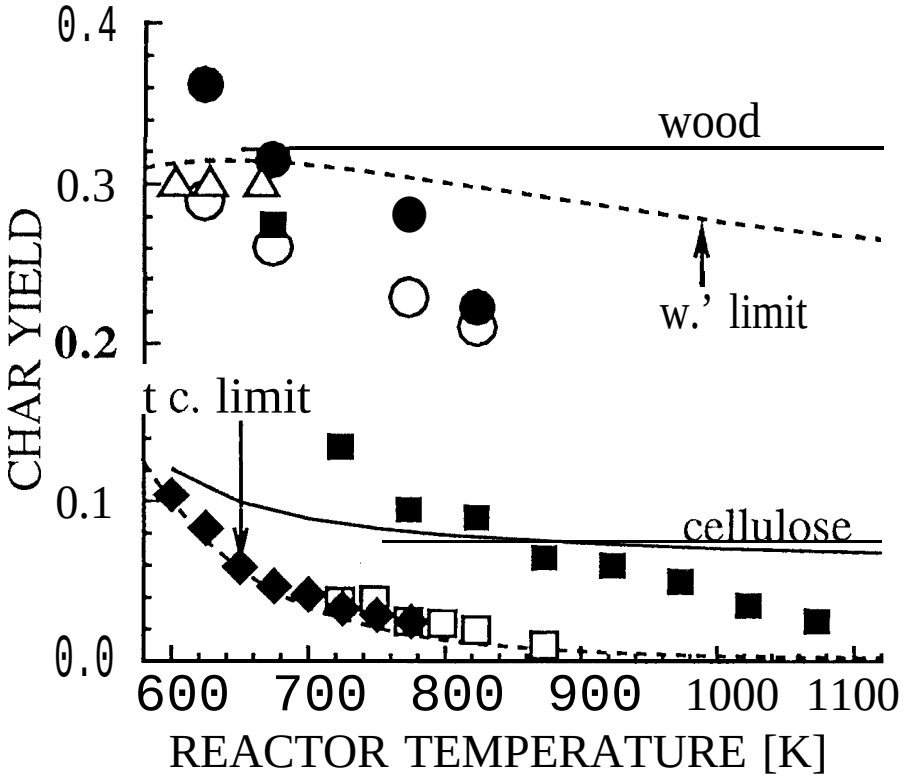
0.4
0.3
0.2
0.1
0.0
CHAR YIELD
wood
w.' limit
t c. limit
cellulose
600
700
800
900
1000
1100
REACTOR TEMPERATURE [K]

Figure 16